Continental Shelf Research
November 2024, Volume 282, Pages 105334 (17p.)
https://doi.org/10.1016/j.csr.2024.105334 https://archimer.ifremer.fr/doc/00911/102302/

Investigating sediment dynamics on a continental shelf mud patch under the influence of a macrotidal estuary: a numerical modeling analysis

Diaz Melanie [1, 2, *], Grasso Florent [2], Sottolichio Aldo [1], Le Hir Pierre [2], Caillaud Matthieu [2]

[1] UMR EPOC, Université de Bordeaux, CNRS, UMR 5805, Bâtiments B18/B18N, Allée Geoffroy Saint-Hilaire, F33615, Pessac Cedex, France
[2] IFREMER - DYNECO/DHYSED, Centre de Bretagne, CS 10070, 29280 Plouzané, France

* Corresponding author : Melanie Diaz, email address : melanie.diaz29@hotmail.com

Abstract :

Shelf mud patches represent major sinks for fine-grained particles on continental shelves, as well as for carbon and contaminants of continental origin. The West Gironde Mud Patch (WGMP) is an interesting example of such offshore marine systems as it is an active mud deposition area located offshore the Gironde estuarine mouth (France) at depths between 30 and 70 m. It is known to be the trap of fine particles coming from the estuary, but the contribution of this material to the total mass of the depocenter is poorly quantified. In addition, despite the economic and ecological issues at stake, the response of such subtidal sedimentary structure to the combination of tidal currents, waves, and river supply remain poorly understood. Thus, using a realistic 3-D hydrodynamic and mixed (mud/sand) sediment transport model, this study aims at investigating the sediment dynamics of the WGMP under different hydrometeorological conditions. The analysis of the residual fluxes at the estuarine mouth exhibited large discrepancies between the different sediment classes as well as for contrasted hydro-and meteorological conditions induced by different dominant transport mechanisms. During winter, the reinforced density gradients drive strong up-estuary baroclinic circulation at the bottom that dominates the sediment dynamics over the barotropic export of mud particles. The model also reproduced the signature of a subtidal mud accumulation area over the continental shelf around 30-40 m water depth, on the proximal side of the observed WGMP. On average over two years, 26% of the mud mass accumulating on the simulated subtidal mudflat comes from the estuary. The trapping efficiency of this mud patch is negatively correlated with the significant wave height. Moreover, due to the estuarine turbid plume being more concentrated and developed at the surface during high river discharge, the trapping efficiency of the mud body is enhanced compared to lower discharge. This study highlights the sensitivity of mud and sand fluxes to vertical and horizontal residual circulation, and points out the uncertainties associated with the simulation of short-term (i.e., years) fine particle deposits compared to long-term (i.e., centuries) sediment accumulation trends. In addition, these results show the primordial effects of both wave action and riverine sediment supply on the dynamics of such subtidal muddy structures, which raises concern about their fate facing climate change and human activities in the future.

Highlights:

► A process-based model simulated mud/sand fluxes along an estuary-shelf continuum ► Density gradients drive up-estuary sand fluxes at the estuarine mouth ► The formation and dynamics of an active shelf mud deposition area are reproduced ► The trapping efficiency of the mudflat is modulated by waves and river turbid plume ► About 26% of the mud mass accumulated on the mudflat originates from the estuary

Keywords : Shelf processes, Estuarine processes, Sediment budget, Sediment flux, Numerical model, Mud patch

1. Introduction

Continental shelves, and more specifically inner-to-mid shelf regions (20-100 m water depth), are key transitional areas located between terrestrial sediment source systems and deep-sea depositional environments (Nittrouer et al., 2007; Nittrouer & Wright, 1994). They are complex areas in terms of sediment dynamics where both continental and marine processes interact (Dalrymple & Choi, 2007). Near major fluvial systems, the inner-shelf sediment dynamics are not only determined by the morphology and climatic conditions of the adjacent shelf but also by the river regime and the intra-estuarine dynamics (Gao & Collins, 2014; Garcia et al., 2013; Latouche et al., 1991). Several processes influenced by the concurrence of tide, river discharge, and wave action occur in these environments and impact the sediment transport along the estuary-shelf continuum (Gao & Collins, 2014).

Continental shelves are generally floored with relict sands and gravels but, off the major active fluvial systems, it is common to observe modern muddy deposits originating from continental sources (Garnaud et al., 2003; Hanebuth et al., 2015; McCave, 1972; Swift et al., 1971). According to McCave (1972), such mud accumulation areas often occur as mid-shelf mud belts bounded landward by highly-energetic storm-dominated reworked sands and seaward by outer-shelves relict sandy sediments. Examples are the Eel shelf mud belt in Northern California (Borgeld, 1987; Sommerfield & Nittrouer, 1999) and the "Grande Vasière" in the Bay of Biscay (Lesueur et al., 2001; Mojtahid et al., 2019; Vanney, 1977).

Isolated mud patches confined in both cross- and along-shelf directions can also be observed on inner shelves at around 50-70 m water depth. Some examples are the Gironde shelf mud patches located seaward of the Gironde estuary mouth in South-Western France (Lesueur et al., 2002), the New England mud patch on the Mid-Atlantic Bight continental shelf (Bothner et al., 1981; Goff et al., 2019) or the Douro and Galicia mud patches on the Northern Iberian shelf (Dias et al., 2002). The formation of such subtidal muddy structures surrounded by sandy sediments differs from the previous ones (*i.e.* mid-shelf mud belts) by their proximity to a continental sediment source and the concurrence of local hydrodynamic components, such as (i) density fronts driven by high sediment concentration in the bottom boundary layer and (ii) boundaries between opposing currents (Hanebuth et al., 2015). They are particularly important ecologically as well as economically as they act as reservoirs of biodiversity, host key benthic habitats, and constitute valuable fishing areas (Azaroff et al., 2020; Odum & Barrett, 1971; Reise, 2001; Temmerman et al., 2013). Moreover, they are considered as one of the most reliable paleo-environmental archives (Bassetti et al., 2016; Hanebuth et al., 2015; Nizou et al., 2010). Their role is crucial not only in fine material circulation but also in determining the fate of continental fine particles and associated contaminants (Gonzalez et al., 2007; Liu et al., 2011; Palanques et al., 1990, 2008). This was for instance highlighted recently by de Mahiques et al. (2016) who found evidence of anthropogenic compounds up to several centimeters below surface deposits in mud depocenters on the shelf off the Santos Estuarine Complex (São Paulo State, Brazil). This suggests not only a strong impact of hydrodynamic events on residual sediment dynamics in these structures but also a significant relationship with suspended sediments coming from continental areas.

Fine particles coming from rivers are the main vectors of nutrients and pollutants such as heavy metals and radionuclides of continental origin. Both estuarine and shelf environments are directly influenced by terrigenous inputs as the particles migrate along the land-sea continuum (Dalrymple & Choi, 2007). Therefore, understanding particulate matter dynamics between estuarine and coastal areas as well as the fate of terrestrial sediment particles on the shelf is of prime interest for environmental purposes such as assessing water quality and monitoring benthic habitats, as well as for economic and social stakes, given the intense anthropogenic activities developing along the coasts (Jay et al., 1997).

Sedimentary records have been widely used to investigate the contribution of both oceanic and continental influences on sediment budgets and to study the impact of different factors (*e.g.* anthropogenic pressures and climate change) on past and modern functioning of the estuarine-shelf system (Azaroff et al., 2020; de Mahiques et al., 2020; Dias et al., 2002; Eckles et al., 2004; Potter et al., 2005). However, given the complexity of processes and the diversity of hydrometeorological conditions occurring in these environments, it is particularly difficult to provide a comprehensive picture of sediment dynamics at a regional scale based on localized sedimentary samples.

In their review of the physical processes driving mud accumulation on coastal shelf environments, Porz et al. (2021) stressed the importance of numerical models to understand the influence of hydrodynamic processes involved. More importantly, numerical modeling appears as one of the most relevant approaches to quantify suspended sediment fluxes at specific locations and at different time scales (Schulz et al., 2018). Such a tool can be used to quantify exchange of material between the continent and the ocean for contrasted hydrometeorological conditions. Simulated residual fluxes provide insights on sediment budgets over the continental shelf (*e.g.* Mengual et al., 2016), and especially on the trapping and dispersive capacity of specific sedimentary structures, such as subtidal mudflats.

The objective of this study is to analyze the behavior of a subtidal mudflat located offshore the Gironde estuarine mouth, the West Gironde Mud Patch (WGMP), which is known to trap particles coming from the Gironde Estuary. More specifically, this work aims at investigating the sediment dynamics of the WGMP in relation to estuarine sediment outflow in order to trace back the behavior of the particles deposited on the mudflat. To do so, it is important as a first step to understand and quantify the sediment fluxes between the estuary and the shelf. Due to the broad range of spatial and time scales involved, quantifying sediment fluxes between an estuary and its adjacent shelf is challenging and has never been achieved before for the Gironde Estuary. In addition, despite ecological issues at stake, existing knowledge on the WGMP dynamics is limited to a study carried out twenty years ago on the origin and morphosedimentary evolution of the mud patch (Lesueur et al., 2002) and to some recent insights on the spatial distribution of surface sediment organic characteristics in this area (Lamarque et al., 2021, 2022). The present-day sediment dynamics over this depocenter are still poorly documented and its behavior in terms of sediment trapping and resuspension associated with the hydrometeorological conditions is still unknown.

For this purpose, a three-dimensional (3D) numerical model of sediment transport over the estuary and its adjacent continental shelf has been developed. The calibration process, along with the validation of the hydrodynamic model and quantification of uncertainties associated with simulated sediment fluxes, has been described in a previous work by Diaz et al. (2020). It provides the validation frame of the multi-class sediment model, which is one of the most complete numerical modeling tools ever developed on this study site, based on a complete realistic description of the estuary and the adjacent shelf. This tool is used in the present study to analyze sediment fluxes between the estuary and the sea, which are computed through two different cross-sections, providing unprecedented insights into the fluxes seasonal and spatial variability. Based on this knowledge, the behavior of the mud patch reproduced by the model is studied for contrasted hydrometeorological conditions, while discriminating the specific contribution of estuarine sediments, to further understand the link between estuarine sediment outflow and sediment dynamics on the continental shelf .

2. Regional setting

This study focuses on the continuum between the Gironde Estuary and its adjacent continental shelf. The Gironde Estuary is one of the largest estuaries of Western Europe, with a 635 km^2-surface area (Jalón-Rojas et al., 2015). It is located on the South-West coast of France on the Bay of Biscay (Figure 1) and results from the confluence of the Garonne and Dordogne rivers. It is 170 km long from the mouth to the upper limit of tidal influence and it drains a watershed surface of about 71,000 km^2 (Allen et al., 1980). The yearly-averaged river discharge of the combined Garonne and Dordogne rivers is about 700 m^3/s (Jalón-Rojas et al., 2015). The Garonne River contributes to about two thirds of the water and sediment discharges into the estuary. There is a well-defined seasonality in the hydrological regime with a high river discharge regime from November to May and a low flow period from June to October. It is one of the two main estuaries supplying the Bay of Biscay in freshwater and sediments. This estuary is defined as macrotidal, with a tidal range of about 1.5 m during neap tides and 5.5 m during spring tides. The hydrodynamics are influenced by strong asymmetrical tidal currents that drive significant sediment tidal pumping (Allen et al., 1980). Gravitational circulation along with tidal pumping and asymmetrical mixing act together to generate one of the most concentrated estuarine turbidity maxima (ETM) in Europe, with suspended sediment concentrations (SSC) in surface waters reaching up to 6 kg/m^3 (Castaing & Allen, 1981; Jalón-Rojas et al., 2015). The seasonal variations in river discharge and salinity intrusion influence the longitudinal excursion of the ETM in the estuary (Allen et al., 1980; Sottolichio et al., 2000): during low river discharge, the ETM migrates upstream in the rivers (Garonne and Dordogne) whereas it moves further downstream during high river flow.

The WGMP is located approximately 30 km to the North-West off the Gironde mouth on a mostly sandy bed (Figure 1b). It consists of a cross-shelf lenticular mud body covering a surface area of about 420 km^2 located between 30 and 75 m water depth. The fine particles coming from the estuary toward the shelf preferentially deposit in this area, as indicated by the biogeochemical analysis of the mud deposits (Lesueur et al., 2002). The formation of this mud body started 2000 years BP by the infilling of a shallow depressed area that crossed the shelf. Sedimentological surveys carried out in the late 1980s highlighted a clear across-shelf distinction between a proximal and a distal area within the WGMP (Lesueur et al., 2002). The characteristics of the deposited sediments as well as the occurrence of sedimentation and erosion events were found to be different between the two parts of the mudflat (borderline around 40-45 m water depth). Lamarque et al. (2021) recently assessed the ongoing validity of this segmentation and further suggested that modern deposition and bioturbation occur exclusively in the distal part. Moreover, sedimentation rates range between 0.1 cm/yr in both the shallowest and the deepest area of the depocenter and 0.5 cm/yr in the central part, around 45-50 m water depth (Lesueur et al., 2001, 2002). The WGMP is also an intensively trawled area mainly for Norway lobsters (nephrops norvegicus, or more commonly called langoustines) and common soles (Lamarque et al., 2021; Mengual et al., 2016).

3. Methods

3.1 Numerical model setup

A 3-D numerical model has been developed to study the hydro- and sediment dynamics along the Gironde estuarine-shelf system. This model has been described in detail by Diaz et al. (2020) who thoroughly quantified epistemic uncertainties associated with the model parameterization and investigated the impact of equifinality on the simulated sediment behavior. Hereafter a brief overview of the model characteristics is provided both in terms of hydrodynamics and sediment transport.

3.1.1 Hydrodynamic model

The model is based on a non-nested (unique) configuration using the hydrostatic model MARS3D (Lazure & Dumas, 2008). An orthogonal curvilinear grid was used to better represent the estuarine shape and to optimize computational costs while refining the grid resolution in some specific areas (*i.e.* in the river meanders, in the central estuary, and at the estuarine mouth) (Figure 1). Horizontally, cell sizes ranged from 40 × 350 m in the meanders to 2 km × 2 km offshore while the vertical grid was divided into 10 equidistant sigma layers (based on Diaz et al. (2020) who studied the influence of the number of vertical layers on the simulated sediment fluxes at the mouth).

The 114 main tidal components, extracted from the CST France database (SHOM), were used to force the circulation at the open boundaries. Surges, provided by a configuration of the MARS2D model applied to a larger domain (*i.e.* over the Bay of Biscay), were added to the water elevation at these same boundaries. Upstream, the realistic Garonne, Dordogne, Isle, and Charente solid and liquid river flows were prescribed. At the surface, the model was forced by wind stresses and pressure gradients obtained from the high-resolution meteorological AROME model (Meteo-France). The simulated turbulence is based on a k-epsilon turbulence closure scheme. Waves were simulated with the WAVEWATCH III® (WW3) numerical model (Roland & Ardhuin, 2014) using the same computational grid as the one used by MARS3D in this study. The free surface elevation and current velocity provided by the MARS3D hydrodynamic model, along with local winds and swell data extracted from a larger model, were used to force the WW3 configuration. Then, the bottom orbital velocities simulated by the wave model were used to compute the wave-induced bed shear stress. The radiation stresses were not accounted for in MARS3D and there was no direct coupling between the hydrodynamic and the wave model. Finally, the total bed shear stress was expressed as a combination of the current-induced and wave-induced bed shear stresses, accounting for non-linear interactions following Soulsby's (1997) formulation. Further details regarding the forcing and the model description are given by Diaz et al. (2020).

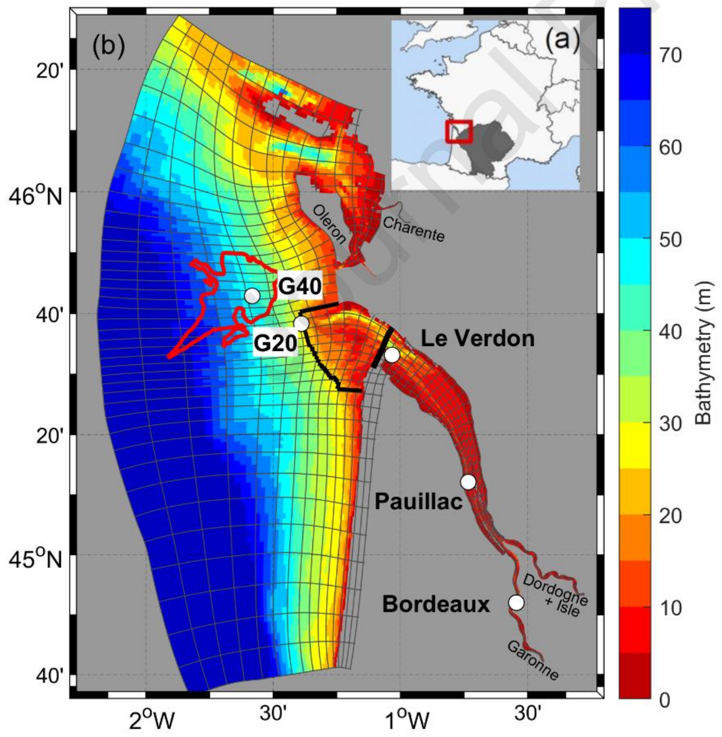

Figure 1 The Gironde fluvial-estuarine system: (a) location map. The gray area indicates the watershed of the Garonne and Dordogne rivers; (b) the bathymetry of the estuary (vertical reference: mean sea level) and its adjacent continental shelf. The gray lines represent the model mesh grid (every fifth cell) and the white circles indicate the measurement stations (where the model is validated, see Section 2.3). Black cross-sections represent the sections through which the fluxes are calculated (the Verdon section upstream the mouth, close to Le Verdon, and the Isobath-25m section offshore the mouth, along the 25m-isobath, close to

the G20 station). The red polygon outlines the contour of the West Gironde Mud Patch (as drawn by Lamarque et al. (2021) based on data obtained during the JERICOBENT-5 cruises (Gillet & Deflandre, 2018; Schmidt & Deflandre, 2018)).

3.1.2 Sediment transport model

The hydrodynamic model was coupled with the process-based, multiclass, multilayer sediment transport model MUSTANG (Grasso et al., 2015; Le Hir et al., 2011; Mengual et al., 2017), which computes the temporal and spatial variations of sand and mud content in the bed under hydrodynamic forces and consolidation process. It also solves the 3D advection-diffusion equations in the water column and the sediment exchanges between the bed and the water column for different particle classes. In this study, five sediment classes were chosen: one gravel, three sands, and one mud (diameters in Table 1). The initial distribution of classes was considered uniform over the entire domain with 10% of gravel, 20% of each sand, and 30% of mud.

Non-cohesive sediment classes (sands and gravel) had constant and uniform settling velocities depending on their diameters (Soulsby, 1997). The coarser classes were transported in the bottom layer only, except for the very fine sand, which was treated in three dimensions. In two dimensions, the velocity in the bottom layer is corrected to account for a logarithmic profile for the velocity in the whole water column, and the calculated sand concentration is then assumed to follow a Rouse profile (Waeles et al., 2007). The mud class was computed as a three-dimensional variable as well with a settling velocity $w_{s,mud}$ varying with concentration and turbulence to represent the flocculation process following Van Leussen (1994):

$$w_{s,mud0} = \min\left[w_{s,max}, \max\left(w_{s,min}\ , c_1 C_{mud}^{c_2} \frac{1+aG}{1+bG^2}\right)\right], \quad (1)$$

with C_{mud} the mud concentration (kg/m^3), G the turbulent shear rate defined as the square root of the energy dissipation divided by the fluid viscosity (s^{-1}), $w_{s,min}$, $w_{s,max}$, a, b, c_1 and c_2 calibration parameters detailed in Table 1. A dependency between the mud settling velocity and salinity (S) was also considered to account for the influence of salinity on flocculation: below a critical salinity of 5 psu, the mud settling velocity decreases with salinity (see details in Diaz et al. (2020)).

The erosion flux was based on the Partheniades-Arathurai equation (Partheniades, 1965):

$$\begin{cases} \tau > \tau_{ce} \ \Rightarrow E = E_0 \left(\frac{\tau}{\tau_{ce}} - 1\right)^n \\ \tau < \tau_{ce} \Rightarrow E = 0 \end{cases} \quad (2)$$

with E the erosion flux, E_0 an erodibility parameter (expressed in kg/m^2/s), τ_{ce} the critical shear stress for erosion (N/m^2) and n a calibration parameter. A distinction between cohesive and non-cohesive sediment behaviors was made based on the mud fraction in the surficial layer of the bed (f_m). In both cases, the Partheniades equation (equation 2) was prescribed with different calibration parameters. For a non-cohesive behavior ($f_m < f_{mcr1}$ where $f_{mcr1} = 1000 * d_{50,sand}$ where $d_{50,sand}$ is the weighted mean diameter of sand classes in the surficial layer), the erosion regime followed a pure sand behavior. The critical shear stress for erosion was determined by the Shields criteria (Soulsby, 1997), the erosion rate was derived from erodibility measurements (Le Hir et al., 2008) (see details in Diaz et al. (2020), Appendix B) and the calibration parameter n is defined as n_{sand} (Table 1). In the presence of a cohesive seabed ($f_m > 0.7$, Le Hir et al. (2011)), the formulation followed a pure mud erosion regime with $n = n_{mud}$ and $E = E_{0,mud}$ (Table 1). The critical shear stress for mud erosion $\tau_{ce,mud}$ was considered varying with the consolidation state of the bed, which is represented by the relative mud concentration C_{relmud} through a classical power law $\tau_{ce,mud} = \alpha_1 C_{relmud}^{\alpha_2}$ (Grasso et al., 2015; Le Hir et al., 2011; Waeles et al., 2008) with α_1 and α_2 defined in Table 1. Here, the relative mud concentration is defined as the mud concentration in the space between sand particles. Finally, for a mixed erosion regime, the erosion law parameters were linearly interpolated between pure sand and pure mud behaviors. All empirical parameters are identified in Table 1 and further details on the formulations used in this model and on the calibration can be found in Diaz et al. (2020).

Table 1 Main sediment model calibration parameters

Particle diameter		*Gravel*	3 mm	*Based on local granulometric data*
		Medium sand	400 µm	
		Fine sand	250 µm	
		Very fine sand	100 µm	
		Mud	30 µm	
Mud settling velocity (eq. 1)		$w_{s,min}$	0.2 mm.s^{-1}	
		$w_{s,max}$	2 mm.s^{-1}	
		c_1	0.006	
		c_2	1	
		a	0.3	
		b	0.18	
Erosion law	Non-cohesive	n_{sand}	1.6	
	Cohesive	n_{mud}	1	
		$E_{0,mud}$	5.10^{-4}	
		α_1	10^{-5}	
		α_2	2	

The deposition flux is calculated using a critical shear stress for deposition for each sediment class which follows the law of Krone (1962) as described in the first place in Le Hir et al. (2011) and later on in Grasso et al. (2018) and Diaz et al. (2020). Moreover, to prevent an excessive increase of bed slope between depositing banks and an eroding channel, the sliding of sediments along the slope is simulated. In MARS3D, this process is computed by assigning a part of the deposition flux from one cell to the neighboring one based on the slope between the two cells. The fraction of fresh deposit transposed to a deeper adjacent cell linearly depends on the local slope.

The calculation of sediment fluxes was performed for every time step during the simulation to ensure sediment mass conservation. Two cross-sections surrounding the estuarine mouth were defined, called

Verdon and Isobath-25m sections (Figure 1), through which fluxes were calculated. These sections were chosen to be representative of the sediments that migrate between the estuary and the continental shelf while discriminating the contribution of sediments of riverine, estuarine, or shelf origin. It has to be noted that the Isobath-25m section also includes two cross-shelf sections on both sides of the estuarine mouth. Thus, even though the along-estuary component clearly dominates the sediment transport in this area (see Figure 20 in the supplementary material), the calculated fluxes at this section also include the along-shelf transport close to the shore. The purpose of this second section was to give a more precise estimation of the total sediment mass reaching the continental shelf or the coastal areas coming from the rivers and estuary, and to distinguish the sediments that are trapped in the estuarine mouth area. Details of the equation solved by the model to compute sediment fluxes are given in Schulz et al. (2018).

3.2 Numerical model validation

The hydrodynamic model has already been validated by Diaz et al. (2020) and provided good skills in terms of water level, current and salinity. Thus, the model validation here is focused on the suspended sediment concentrations (SSC), which is the main interest of the present work. As the first step of this study is to evaluate sediment fluxes at the mouth and to investigate sediment dynamics on the adjacent continental shelf, a supplementary validation analysis is conducted hereafter to assess model validity further offshore than has been done previously by Diaz et al. (2020). For this purpose and based on their results, the calibration parameters (detailed in Section 2.2) have been adjusted to improve the simulated sediment dynamics at the mouth and on the continental shelf.

Diaz et al. (2020) performed a large number of model simulations with different parameter sets as part of the calibration process of the MARS3D Gironde curvilinear model (same as used in this paper). Following a methodology based on equifinal parameter sets (*i.e.* different combinations of model empirical parameters resulting in equivalent skills when compared with SSC measurements (Beven, 1993; van Maren & Cronin, 2016)), they assessed the uncertainties on simulated sediment fluxes at the mouth associated with such complex 3D process-based models. Based on their results, the aim of the supplementary calibration conducted for the purpose of the present study was to identify the set of parameters that would bring together the best model performances while ensuring a reasonable estimation of sediment fluxes at the mouth. To do so and for a proper comparison, the model skills were evaluated with the same method, *i.e* the target diagram methodology (see Diaz et al. (2020) or Jolliff et al. (2009) for more details), on simulations of the year 2015 after a one-year spin-up. As a result, the mud erodibility has been increased through the mud erosion parameter (0.0005 instead of 0.0003) while increasing the lowest limit of the mud settling velocity (0.2 instead of 0.1 mm/s). This new parameterization enabled to maintain good model skills (normalized RMSE of 0.93, see more details on the formulation used in Diaz et al (2020)) while limiting mud export at the mouth (around 2.9 Mt/yr at the Verdon section). This export of fine particles was more in line with what is expected on the long term to balance the amount of mud supplied by the rivers (around 1-2 Mt/yr) compared to Diaz (2019) (around 7 Mt/yr exported at the mouth).

With this new set of parameters (see Table 1), realistic simulations of years 2016 and 2017 (*i.e.* with observed meteorological, hydrological, and tidal forcing) were carried out. Those two years were chosen because SSC measurements were available for validation both in the estuary and on the adjacent continental shelf during this period and they were also well representative of contrasted hydro-meteorological conditions. To ensure the relevance of the analysis, the numerical model results (*i.e.* years 2016-2017) were obtained after a 5-year spin-up using realistic forcing of the year 2015. This means that the year 2015 was simulated 5 times with the same hydrometeorological forcing and that the final state of each year, in terms of both SSC and sediment bed composition, was used as the initial state for the following year. This allows the model to redistribute the initially uniform sediment coverage and to reach an equilibrium state in terms of both sediment fluxes at the mouth and sediment bed composition. This equilibrium state was assessed by comparing a sixth simulated year with the fifth (see figures 15 and 16 in supplementary data). It also enables to reach a realistic suspended sediment mass within the ETM (between 2 and 4 Mt depending on the tidal range, see figure 17 in supplementary data, fitting the estimation found in the literature, *e.g.* Jouanneau & Latouche (1981))

Numerical model results were validated using intra- and extra-estuarine in-situ measurements of SSC as reference data. Intra-estuarine SSC data were provided by the Gironde continuous monitoring network of estuarine water quality (MAGEST, Etcheber et al. (2011); Schmidt et al. (2016)), which measures turbidity 1-m below the surface. Supplementary validation data were obtained on the adjacent continental shelf from the two Gironde Estuary Mouth MEasurement Stations (GEMMES) in the frame of the METEOR research cruises (Grasso, 2017; Grasso et al., 2021): (i) in front of the estuarine mouth around 20-m water depth, surface SSC was measured (station G20, Figure 1); and (ii) in the WGMP around 40-m water depth, bottom SSC was recorded 1-m above the bed (station G40, Figure 1). These extra-estuarine measurement stations were deployed during approximately one year between November 2016 and October 2017 (with scattering due to technical problems in the measurements, see Figure 2d and e).

The model ability to reproduce the measured behavior of SSC has been quantified (Table 2) over the whole measurement period available at each station and for hourly data with the correlation coefficient R, the Root Mean Square Error (RMSE), and the Willmott's (1981) skill score (an index of 1 indicates a perfect agreement while an index of 0 means no correlation between the two variables, more details in Appendix A). In addition to this index, the magnitude of the RMSE describes the average deviation between the model results and the observed data. Moreover, the validation of model results was also carried out by assessing the model ability to reproduce observed SSC trends as a function of river discharge for the intra-estuarine stations (*i.e.* Pauillac and Bordeaux), and as a function of significant wave height (H_s) for the extra-estuarine stations (*i.e.* G20 and G40 stations), where SSC was mainly driven by wave action (Figure 3). Given the limited sampling period of G20 and G40 measurements off the estuarine mouth (*i.e.* 1-6 months, see Figure 2), the relationship with river flow was not relevant enough and showed no clear tendencies on the measuring period.

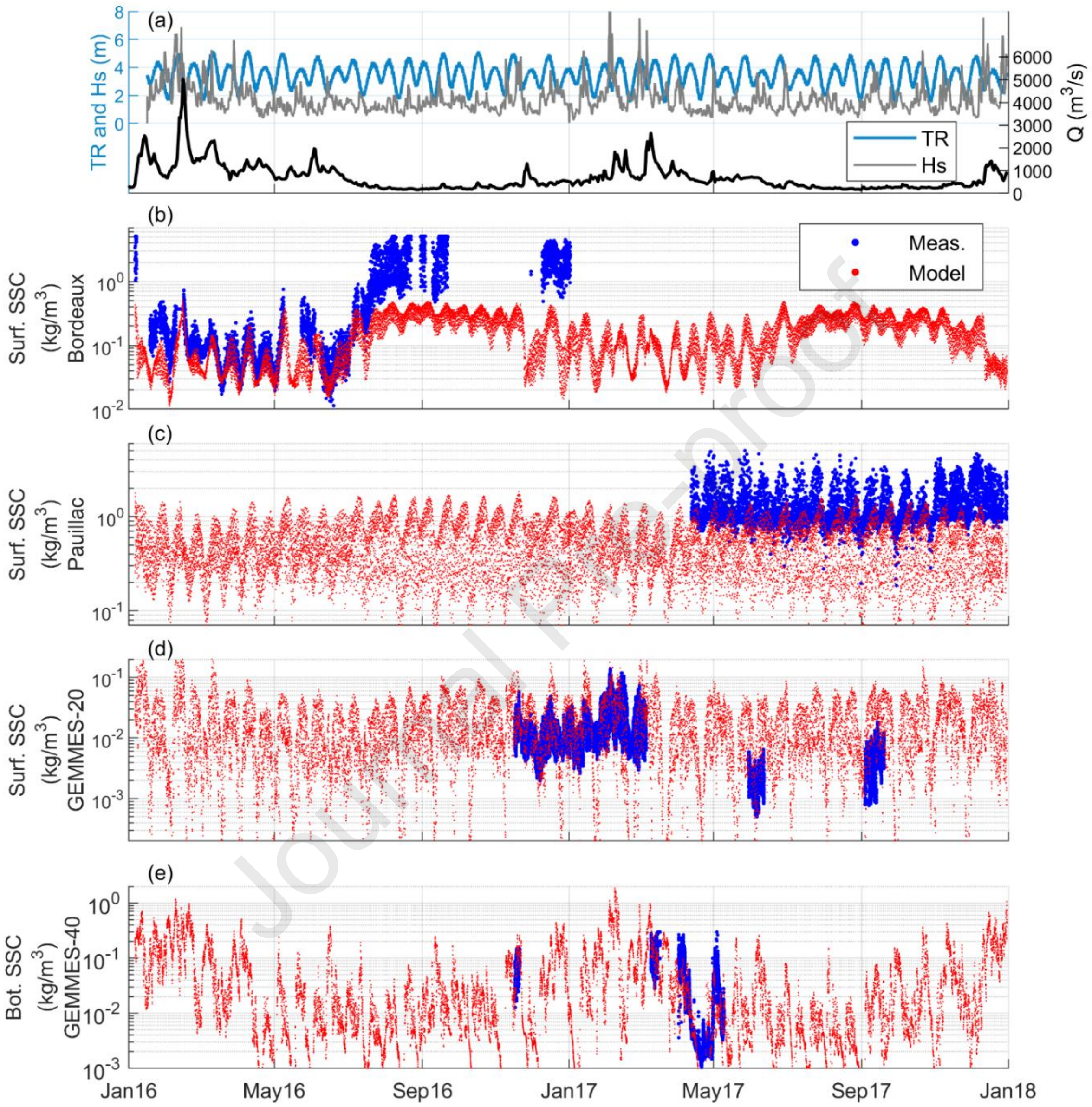

Figure 2 SSC dynamics over the years 2016 and 2017 shown on a logarithmic scale. (a) Tidal range at the estuarine mouth (blue, station Le Verdon), significant wave height Hs on the inner shelf (gray, station G40), and cumulated Garonne and Dordogne river flow Q measured upstream the rivers (black). (b, c, d, and e) Time series of measurements (blue) and model outputs (red) of suspended sediment concentrations for the years 2016 and 2017 1 meter below the surface at (b) Bordeaux, (c) Pauillac and (d) G20 stations, and (e) 1 meter above the seabed at G40 station. Turbidimeter saturation can be noticed at Bordeaux during the summer of 2016. (see Figure 1 for locations)

Table 2 Skill scores computed at the four measurement stations on the SSC parameter

Station	Correlation coefficient R	RMSE (kg/m^{-3})	Willmott's (1981) skill score
Bordeaux	0.65	1.35	0.43
Pauillac	0.23	0.96	0.45
G20	0.49	0.02	0.61
G40	0.49	0.07	0.7

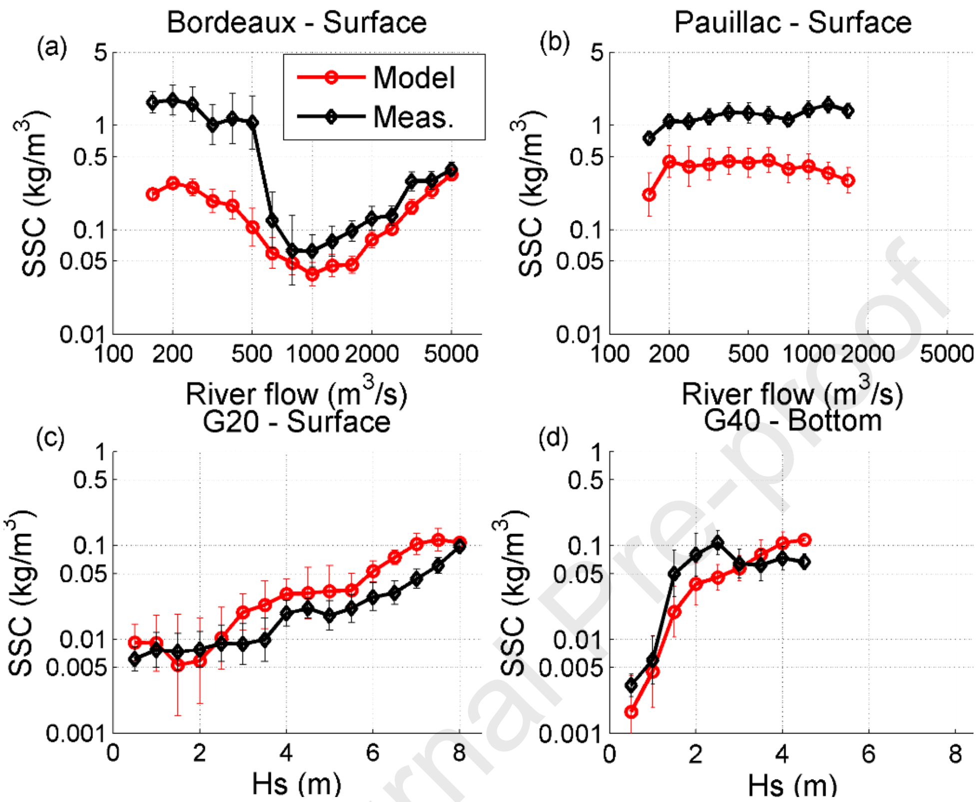

Figure 3 Comparisons of (black) observed and (red) simulated (a, b, c) near-surface and (d) near-bottom SSC seasonal trends associated with (a, b) the river discharge Q and (c, d) the significant wave height Hs at the four measurement stations (a: Bordeaux, b: Pauillac, c: G20 and d: G40, see Figure 1 for locations). Lines and symbols represent data average associated with the considered river discharge ranges (0.1 of log10(Q)) or Hs classes (every 0.5 m). Vertical bars stand for data instantaneous standard deviation (i.e., with no tide averaging) within the river flow or Hs class. Results are plotted on a logarithmic scale, except for the significant wave height axis (c and d x-axis).

In the estuary, the measured SSC dynamics are strongly modulated by river discharge (Figure 3a and b, black lines, see also Figure 18 in supplementary material). When the river flow decreases, SSC increases at Bordeaux and decreases at Pauillac as the ETM migrates upstream. Conversely, when the river flow increases, the ETM shifts downstream and SSC decreases upstream while increasing in the central estuary. Finally, at Bordeaux station, after reaching its lowest value for a river discharge of around 1000 m^3/s, SSC increases again with the river flow due to the high concentrations of particles transported during strong flood events. It should be noted that the Pauillac station was replaced in 2016 and started measuring again in April 2017. Thus, the high river flow conditions were poorly represented at this location (Figures 2c and 3b).

At Bordeaux station, the model reproduces reasonably well the seasonal SSC dynamics associated with river flow (Figure 3a), as well as the fortnightly tidal signal (Figure 2b). The large correlation coefficient (R=0.65, Table 2) indicates that the physics of the ETM migration in this area is well reproduced by the model. Despite large differences in magnitude (RMSE=1.35 g/l, Table 2) due to an underestimation of SSC during low river flow (*i.e.* in the ETM), the sediment dynamics are very well simulated for river flow higher than 800 m^3/s (Figure 3a). In the central estuary (Pauillac station), the model also underestimates the ETM suspended concentrations (Figures 2b and 3c). The discrepancies between simulated and measured SSC are quite large at Pauillac station (RMSE = 0.96 g/l and R=0.23, Table 2). The same issues have already been encountered by many authors while setting up a numerical model of sediment transport in this estuarine system (Orseau et al., 2020; van Maanen & Sottolichio, 2018). However, as inferred by Diaz et al. (2020), this underestimation might be the consequence of a lack of representativeness by the measurements of the turbidity lateral variability in the estuary. Moreover, local resuspensions at Pauillac station are likely to increase measured turbidity levels locally and may not be fully captured by the model due to the coarse grid cells. However, the model manages to capture the neap/spring tidal phasing which ends up in a reasonable value of Willmott's index of agreement of 0.45 (Figure 2c).

As the purpose of this study is to investigate the sediment dynamics at the estuarine mouth and offshore, the validation and calibration of empirical parameters were focused on the G20 and G40 stations. At both stations, the observed signal showed strong sediment resuspension during energetic conditions, which was very well reproduced by the model (Figure 2d, e and Figure 3c, d). The averaged deviations between model results and measurements are low (RMSE < 0.1 g/l, Table 2) and the Willmott's agreement index is very good: at G40, it is comparable and even better than the performance of models used recently to study the sediment transport in other estuaries (Dunn et al., 2015; van Maanen & Sottolichio, 2018; van Maren et al., 2015; Zhang et al., 2019). Such good agreements between measured and simulated SSC at the estuarine mouth provide a reasonable level of confidence in the model capacity to properly simulate sediment fluxes between the estuary and the continental shelf.

4. Results

4.1 Sediment fluxes at the mouth

The simulated sediment exchanges are illustrated with time series of cumulative fluxes through the chosen cross-sections and are defined as positive up-estuary and negative seaward. For each considered sediment class, simulated fluxes showed very contrasted behaviors (Figure 4).

At the upstream river mouth (Verdon section, Figure 1), the residual transport after 2 years is directed offshore for mud, fine sand, and medium sand classes (-5.7 Mt, -1.8 Mt and -0.2 Mt, respectively) and directed upstream for very fine sand and gravel classes (+6.4 Mt and +0.4 Mt, respectively) (Figure 4a).

The three sand classes, and especially the very fine sand, exhibit strong seasonal dynamics associated with river discharge. During high river flow, the sand residual fluxes are directed toward the estuary. However, during low river flow, while the very fine sand residual flux is almost zero, the fine and medium sands are exported offshore, which compensates for the residual import during winter and ends up in a residual export over the year. As for the mud class, its dynamics is significantly influenced by the neap/spring tidal cycle (fortnightly increase/decrease in export of mud, blue line in Figure 4a). Mud fluxes are directed offshore all year long, except during winter episodic stormy events. During these, the otherwise stable export of mud is slightly slowed down by the reinforcement of the baroclinic circulation induced by large river flow, which increases upstream sediment transport. The influence of these stormy events is difficult to distinguish from the impact of high river discharges (*i.e.* ETM shifting downstream and reinforcement of the baroclinic circulation) due to their concomitance.

Contrasted hydrological regimes between 2016 and 2017 resulted in different annual residual fluxes for mud and sand classes at the Verdon section. During the wetter year 2016 (mean annual river discharge of 804 m^3/s), the export of mud and import of very fine sand are stronger than during the dryer year 2017 (mean annual river flow of 572 m^3/s): -3.2 Mt/yr *vs* -2.5 Mt/yr for mud and +3.7 Mt/yr *vs* +2.7 Mt/yr for very fine sand, during 2016 and 2017 respectively. Conversely, for coarser particles, the trend is reversed with stronger export in 2017 than in 2016 (-0.6 Mt/yr in 2016 *vs* -1.2 Mt/yr in 2017 for fine sand and a residual import of medium sand of +0.1 Mt in 2016 *vs* a residual export of -0.3 Mt in 2017).

At the offshore cross-section (Isobath-25m section, Figure 1), the model simulates a residual flux over two years directed offshore for mud and fine sand (-4.5 Mt and -1.55 Mt, respectively) and directed up-estuary for very fine sand, medium sand and gravel classes (+1.4 Mt, +0.85 Mt and +1.76 Mt, respectively) (Figure 4b). This represents the amount of sediment actually exchanged with the coastal ocean, which is strongly influenced by the neap-spring cycle (especially for fine particles), the seasonal dynamics associated with river flow, and the wave action. In this area, both high river discharge and waves, which almost occurred simultaneously during winter, act in favor of a strong import of fine particles toward the estuarine mouth (mud and very fine sand). Conversely, low river discharge and quiescent conditions imply a residual export of fine sediments. Coarser sands tend to be influenced by both the river flow, *i.e.* by the density-induced circulation, and the wave conditions: they tend to be imported toward the estuary with high river discharge (early 2016) and exported when energetic wave events occur. The large variability observed in sediment fluxes associated with the different classes is further discussed in Section 5.2.

Residual fluxes after two years of simulation exhibit a loss of mud from the estuary toward the ocean of about 5.7 Mt (blue line, Figure 4a), including 1.2 Mt trapped in the estuarine mouth (5.7 Mt entering at the Verdon section minus 4.5 Mt leaving at the Isobath-25m section, blue lines in Figure 4a and b).

Conversely, residual fluxes of very fine sand display a loss of about 5 Mt from the mouth toward the estuary (red line, Figure 4a) despite an input of about 1.4 Mt from the adjacent continental shelf (red line, Figure 4b). Finally, the model simulates a residual storage of coarser particles into the estuarine mouth after the two simulated years (black, green, and pink lines, Figure 4a and b).

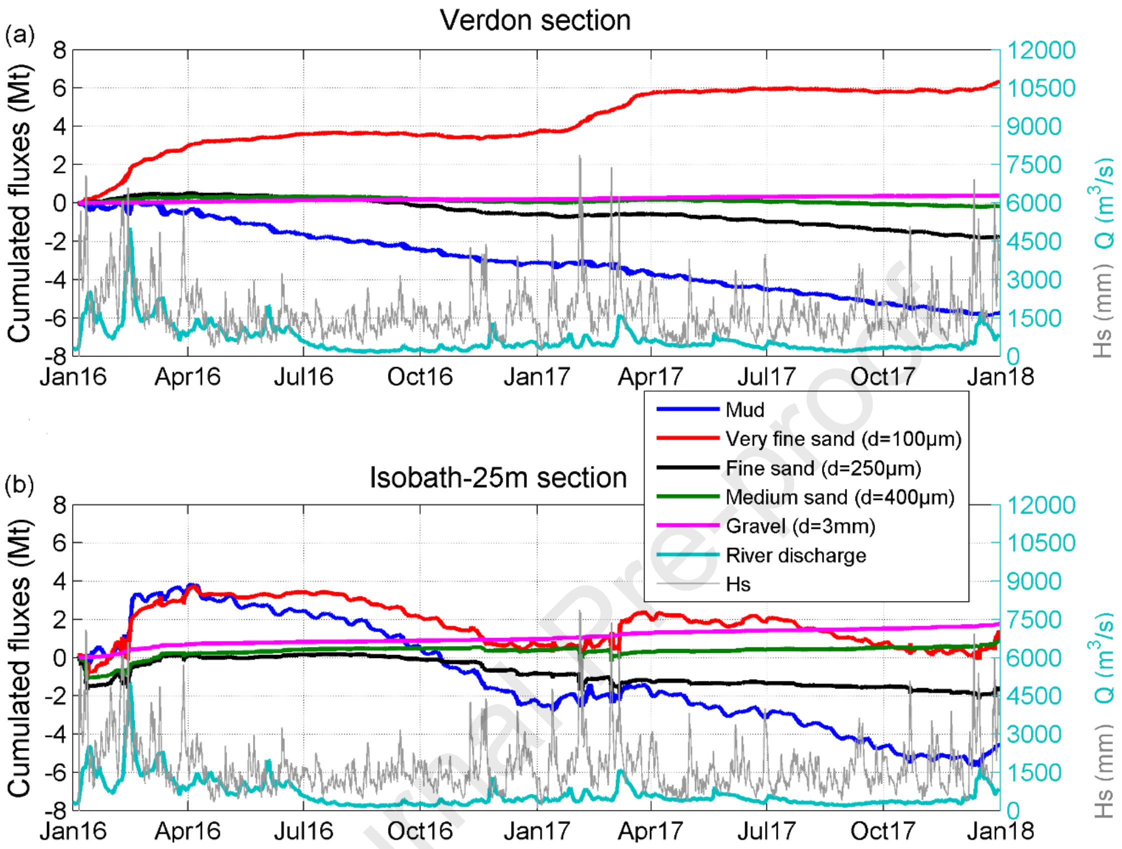

Figure 4 Time series of cumulative fluxes of each sediment class across section (a) Verdon and (b) Isobath-25m (see Figure 1 for locations) along with the cumulated Garonne and Dordogne discharge time-series (right axis, cyan line) and the significant wave height at station G40 (right axis, gray line, see Figure 1 for location). Positive fluxes indicate up-estuary transport and negative fluxes indicate sediment export toward the continental shelf.

4.2 Accumulation and dispersion areas on the adjacent shelf

The residual sediment coverage after 7 years of simulation (5-year spin up + 2016 and 2017) is represented using each class fraction in the surficial sediment (averaged over a thickness of 11.6 cm, corresponding to the storage of model results during the simulation, Figure 5) and their total mass (Figure 6). The surficial sandy sediments are sorted by grain size with coarser particles on the shore, where the wave action is dominant, and finer sandy particles offshore (Figure 5b to 5e). In the estuarine mouth, where the conditions are highly energetic, the dominant surficial particles are medium sands and gravels. However, as can be seen from Figure 6b, the remaining sediment mass is very small in this area and almost the whole initial sediment stock has been eroded, except for lateral banks. Moreover, sandy particles accumulate at the outlet of the two channels of the Gironde mouth, at around 20 m water depth (Figures 5b, c, d and 6b).

The mud distribution tends to be patchier (Figure 5a). An accumulation area of mud is simulated to the North-West of the mouth around 30-40 m water depth, where the mud fraction in surficial sediment and the depth-integrated mass are exceeding 40% (Figure 5a) and 2000 kg/m^2 (Figure 6a) locally, respectively. It is located to the North-East of the currently active WGMP as represented by Lamarque et al. (2021). It is arbitrarily delimitated by a box (blue rectangle, Figure 5a) in order to investigate the response of sediment dynamics to hydrometeorological conditions over this integrated area.

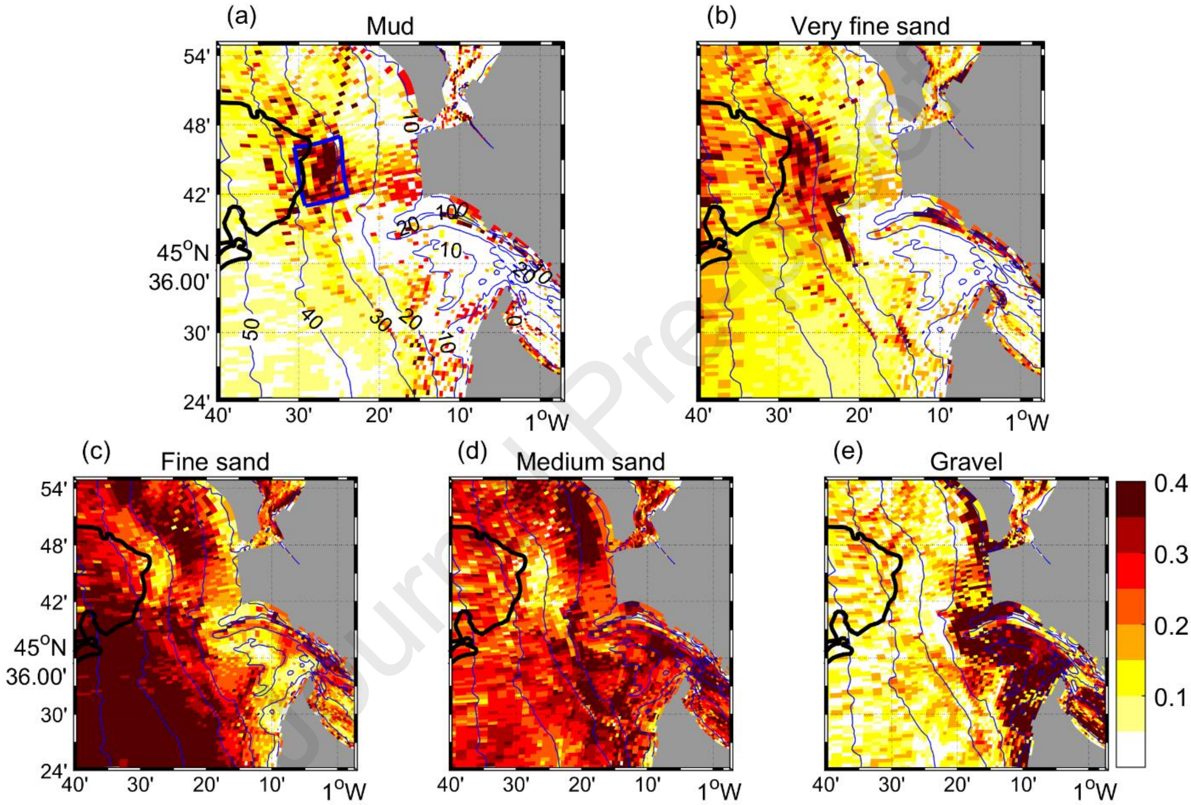

Figure 5 Fraction of each sediment class in the surficial sediment (11.6 cm) from a to e from finer to coarser grain size at the end of 2017. Blue contours are delimitating isobaths every 10 m (vertical reference: mean sea level). The black shape outlines the contour of the West Gironde Mud Patch (as drawn in Figure 1 based on Lamarque et al. (2021)). In (a), the blue box represents the mud accumulation area.

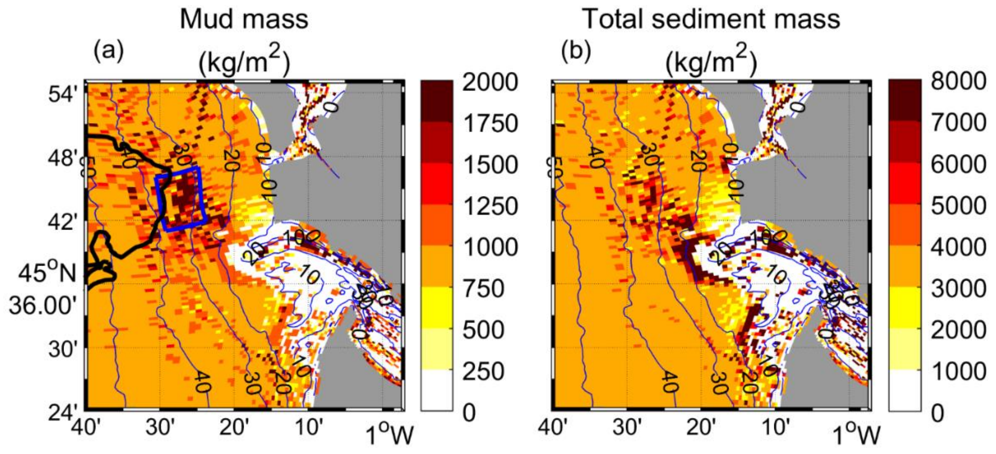

Figure 6 (a) Mud and (b) total sediment mass distribution maps at the end of 2017. Blue contours are delimitating isobaths every 10 m (vertical reference: mean sea level). The black shape outlines the contour of the West Gironde Mud Patch (as drawn in Figure 1 based on Lamarque et al. (2021)). In (a), the blue box represents the mud accumulation area as determined from Figure 4a. The initial mass of mud and total sediment were 1080 and 3600 kg/m2 respectively.

To improve the understanding of mud particles behavior, three different classes of mud were defined based on their origin, *i.e.* their location after the spin-up period, at the beginning of 2016: shelf, estuarine and riverine mud. The distinction between shelf and estuarine mud is considered at the Verdon section (Figure 1) and the riverine mud corresponds to the particles supplied by the rivers during the 2016-2017 simulations (*i.e.* no riverine mud at the beginning of 2016 in the domain). Note that, following this consideration, the mud particles located in the mouth area between the two sections are marked as shelf mud.

At the upstream river mouth (Verdon section, Figure 1), the residual fluxes over two years of estuarine and riverine mud are directed offshore and are about -12.9 Mt and -0.16 Mt respectively, while there is an import of about 7.3 Mt of shelf mud into the estuary (Figure 7a). About 66% of this exported estuarine mud and 59% of the fluvial mud, *i.e.* -8.5 Mt and -0.10 Mt respectively, are further exported toward the continental shelf through the Isobath-25m section (Figure 7b), which means that about one-third of the mud leaving the estuary is temporarily stored in the estuarine mouth. Moreover, a residual flux after two years of about 4.1 Mt of shelf mud is imported into the estuarine mouth (Isobath-25m section, Figure 7b), which means that about 44% of the mud imported into the estuary is coming from the mouth area.

The dynamics of the shelf mud flux exhibits a strong seasonal signal associated with river discharge and strongly modulated by wave action, especially through the 25m-isobath. There is a strong import of shelf mud toward the estuarine mouth during high river discharge period compensated by a mud flux directed offshore during the dry season, itself reinforced by stormy conditions (late 2016 period, Figure 7b).

The vast majority of the mud deposited on the continental shelf after two years of simulation was already originally present on the shelf (Figure 8a). However, in the estuarine mouth area, along the two channels of the Gironde mouth, there is a large part of the deposited mud originating from the estuary (up to 30% at the outlet of the Northern channel). However, as shown in Figure 6a and b, the estuarine mouth is a very energetic area where almost the whole initial stock of sediment has been eroded. Therefore, the mud fraction in this area does not represent a large sediment mass. Further to the North-West, between 30 m and 40 m water depth off the Oleron Island (see the location of the island in Figure 1) and over the simulated WGMP, the estuarine mud signature is still significant (between 5 and 10% of the total mud mass in the surficial sediment, Figure 8b), which is corroborated by observations by Lesueur et al. (2002).

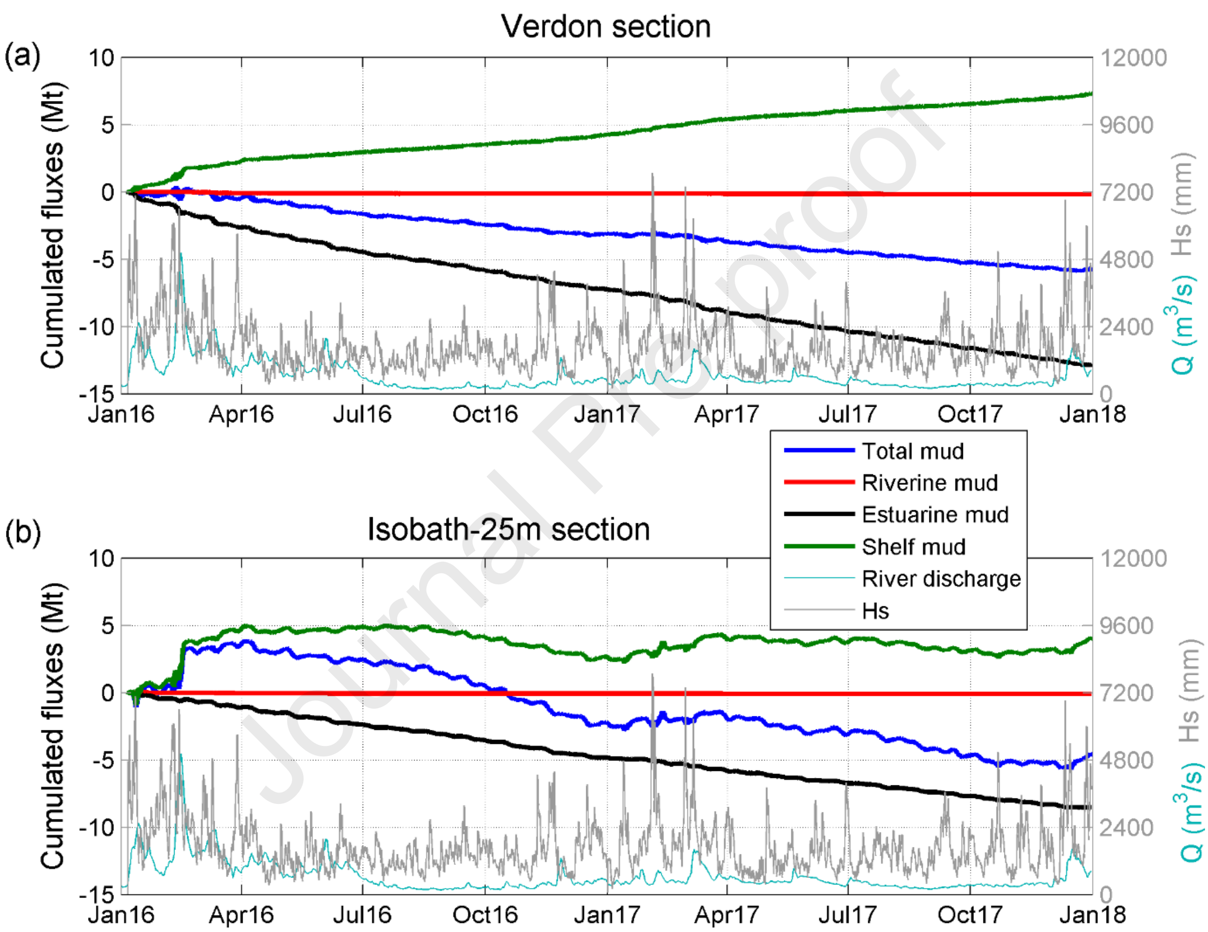

Figure 7 Time series of cumulative fluxes of each mud class across section (a) Verdon and (b) Isobath-25m (see Figure 1 for locations) along with the cumulated Garonne and Dordogne discharge time-series (right axis, cyan line) and the significant wave height at station G40 (right axis, gray line, see Figure 1 for location). Positive fluxes indicate up-estuary transport and negative fluxes indicate sediment export toward the continental shelf.

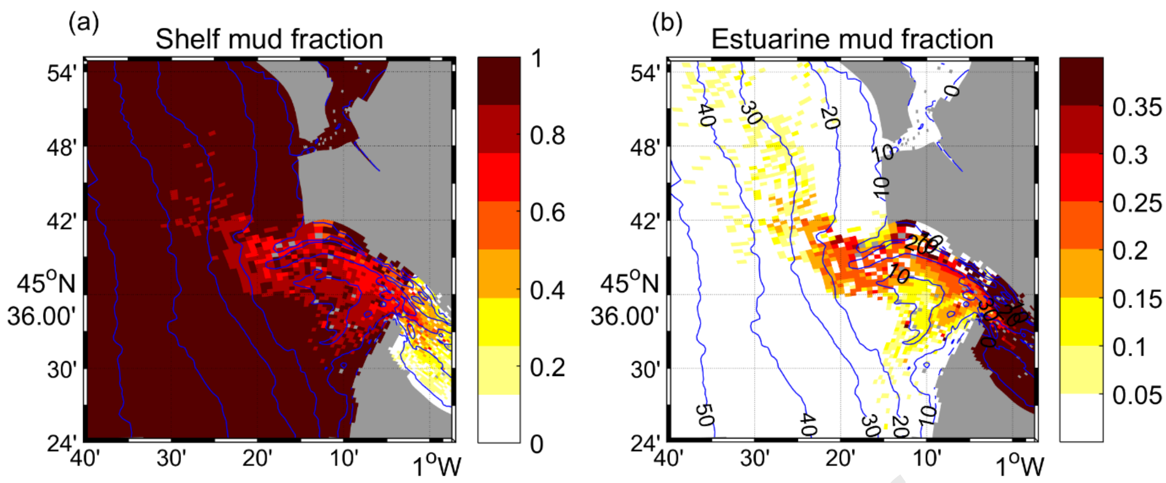

Figure 8 (a) Shelf and (b) estuarine mud fractions in the surficial mud mass (11.6 cm). Blue contours are delimitating bathymetric contours every 10 m (vertical reference: mean sea level).

4.3 Sediment budgets in subtidal mudflats under estuarine influence

Even if the model does not reproduce the contours of the mapped WGMP, it simulates a subtidal accumulation area of mud close to the observed one. The dynamics of this simulated mud deposition area are investigated in this section. To study the influence of hydrometeorological conditions and understand the behavior of this mud depocenter, sediment mass and bed level time series are integrated over the simulated mud body, which is defined as the area within the blue box in Figure 5a. The quantities are then monthly-averaged (Figure 9a-e) and changes from one month to another are represented in Figure 9f.

On average, over one year, sediments are accreting in this area, with a residual erosion during winter (*i.e.* high river discharge associated with energetic meteorological events) compensated by a strong accumulation of particles during dry and quiescent conditions. The sedimentation rates are overestimated by the model with a mean rate of about 4 cm/yr (Figure 9c), which is an order of magnitude larger than the rates measured by Lesueur et al. (2002) (between 0.1 and 0.4 cm/yr). After two simulated years, the accumulation area is mainly composed of mud (6.5 Mt, *i.e.* 64 % of the 10.1 Mt of total mass accumulated on the area), very fine sand (1.9 Mt, *i.e.* about 19% of the total mass), and fine sand (about 1.6 Mt, *i.e.* 16% of the total mass) (Figure 9d).

74% of the mud mass accumulated in this area in two years originates from the adjacent continental shelf (about 4.8 Mt) (Figure 9e). The other 26% (1.7 Mt) are coming from the estuary. Strong mud erosion occurs during winter energetic conditions compensated by residual accretion during the rest of the year (Figure 9f). Similarly, the very fine sand is strongly resuspended during winter and accumulates otherwise, while the fine sand is less mobilized (Figure 9d).

To better visualize the response of the mud body to hydrometeorological conditions, the mud mass changes per month (represented in Figure 9f) are plotted against the monthly mean wave-induced bottom shear stresses, with the monthly mean river discharge in color in Figure 10. The mud mass evolution is negatively correlated with wave action and the mudflat mostly undergoes accretion for wave-induced bed shear stresses lower than 0.3 N/m^2. Moreover, during high river discharge, the trapping efficiency of the mud body is enhanced compared to lower discharges.

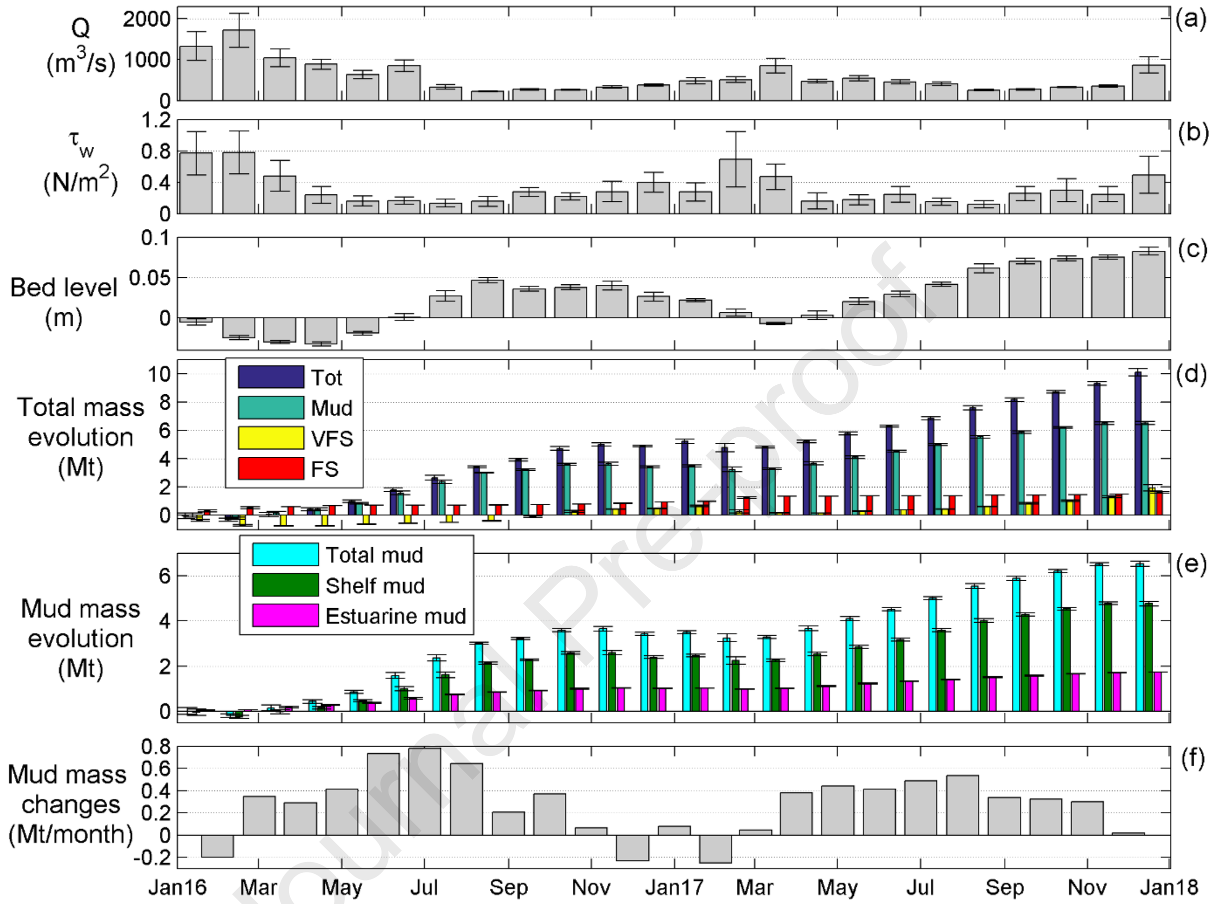

Figure 9 Variability of forcing and sediment mass in the simulated subtidal mudflat represented by the blue box in Figure 4a during 2016 and 2017. Monthly mean and standard deviation of (a) river discharge, (b) bottom wave-induced shear stress, (c) bed level, (d) mass evolution of total sediment and each significant class of sediment, and (e) mud mass evolution distinguished by its origin. (f) Monthly mud mass changes.

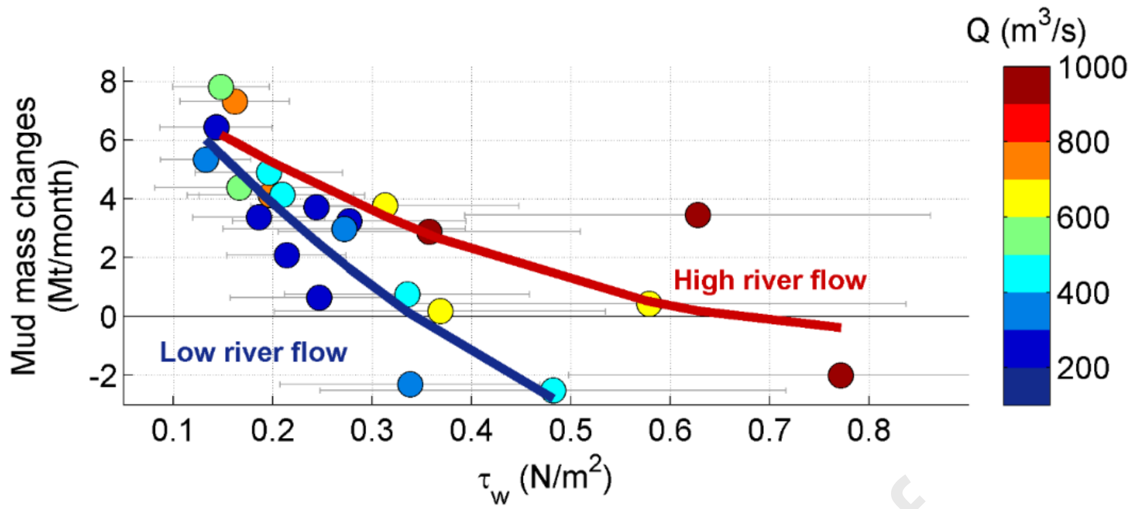

Figure 10 Relationship between the monthly-averaged wave-induced bottom shear stress and the monthly mud mass change for different hydrological conditions (colors). The blue and red polynomial fit curves were calculated for river discharge conditions below and above 500 m3/s, respectively.

5. Discussion

5.1 Sediment transport processes along the land-sea continuum

Many studies using numerical models have already been carried out to investigate the Gironde Estuary sediment dynamics (*e.g.* Li et al., 1994; Sottolichio et al., 2000; Van, 2012). For instance, van Maanen & Sottolichio (2018) applied a 3D hydrodynamic and sediment transport model to study the response of the ETM to changes in river discharge and mean sea-level. More recently, Orseau et al. (2020) used a different sediment transport model to reproduce the estuarine mixed sediment dynamics in a two-dimensional depth-averaged framework. However, to the best of the authors' knowledge, the current study is the first attempt to simulate the three-dimensional mixed sediment transport from riverine to shelf environments in this system. This tool was thought to be as efficient and robust as possible. It has been calibrated to reproduce the sediment dynamics near the mouth and over the adjacent continental shelf while preserving the model performance in the central and upper estuary. For the first time on this study site, a 3D numerical model of mixed sediment transport is capable of simulating sediment dynamics over a multiannual time scale (7 years of simulation) and an extended area offshore the estuarine mouth with a satisfactory validation state.

The sediment transport in the Gironde Estuary is mainly driven by both tidal forcing and density gradients. Tidal asymmetry plays a major role in the formation of the ETM while density gradients act to stabilize its mass by limiting sediment export offshore (Castaing & Allen, 1981; Sottolichio et al., 2000; van Maanen & Sottolichio, 2018). Regarding the sediment transport toward the continental shelf, the Gironde turbid plume has been described by satellite images, revealing that it is more concentrated and spreads further offshore during high river flow (Constantin et al., 2018; Froidefond et al., 1998). This might lead to the general idea that the Gironde Estuary exports more fine sediments to the ocean during high river flow period. However, the results of this study revealed that, as the stratification intensifies with the river flow, the up-estuary baroclinic-induced circulation becomes the dominant mechanism for sediment transport at the mouth. As it can be seen in Figure 4, it acts to slow down mud export while driving strong import of very fine sand into the estuary. The weaker stratification during the dry season implies a reduced density circulation and an enhanced seaward residual transport of fine sediment. Thus, an important result from this study is that satellite data should be used very carefully to derive sediment export from estuaries.

An important feature in this system, as in most macrotidal estuaries around the world, is associated with the longitudinal and lateral structure of the residual sediment transport. To the best of the authors' knowledge, this remains uninvestigated in the Gironde estuarine mouth. Even if the analysis of the horizontal structure of the sediment transport is considered out of the scope of this work, a quick review of some horizontal and vertical structures seen in the model results is given in section 5.2 in order to explain more in details the differences in sediment fluxes for the different classes. Also, a recent study carried out by Alahmed et al. (2021) emphasized the very complex characteristics of both along-channel and lateral residual (water) circulation near the estuarine mouth. Such residual flows associated with density gradients, advection, and mixing are most probably the drivers of the residual sediment transport highlighted in this study. An interesting step toward improving our understanding of sediment fate between the estuary and the continental shelf would be to investigate the dominant mechanisms driving sediment transport at the mouth and how they relate to the lateral and longitudinal residual flows.

5.2 Sediment flux estimate and its associated uncertainties

Although it is one of the two main sources of fine sediment supplied to the Bay of Biscay, the few studies that have tried to provide an estimate of fluxes at the estuarine-shelf interface in the past are quite old and inaccurate, given the very few measurements and sampling period considered (Castaing & Jouanneau, 1987; J. M. Jouanneau et al., 1999). The numerical model used in this study has been developed to provide this knowledge as accurately as possible. Prior to the results presented here, Diaz et al. (2020) conducted a model sensitivity analysis and quantified the uncertainties associated with the sediment fluxes to be around 93% for mud and 51% for sands and gravel together. A modeling effort has also been made to address the issue of the spin-up period. As revealed by the supplementary data (Figures 15 and 16), for the sedimentary patterns and fluxes to stabilize and reach an equilibrium, 5 spin-up years were necessary before diving into any analysis of the results. This issue should not be left aside as it can have a significant impact on the simulation results (Diaz et al., 2020).

The simulated sediment dynamics between the estuary and the ocean exhibited large discrepancies between the different sediment classes (Figure 4). On average over the two simulated years, there is a residual export of mud and fine sand toward the ocean through the 25m-isobath and a residual import of very fine sand, medium sand, and gravel toward the estuarine mouth. At the upstream mouth (Verdon section, Figure 1), the mud along with the two coarser sands are exported toward the mouth whereas the very fine sand and gravel residual fluxes are directed upstream.

Such different behavior can be explained by different mechanisms. First of all, it should be noted that the very fine sand is the only sand class treated as a three-dimensional variable in the model. The other two coarser sands and the gravel are treated in two dimensions, as they are essentially transported near the bed: their advection is computed based on the near-bed velocity only. This surely promotes different behaviors than the mud and very fine sand classes, which can be transported along the whole water column. Moreover, the dominant dynamics between mud and sands transport are inherently different, as the mud tends to be advected both close to the bottom and with surface waters. In the meantime, sand particles are usually transported near the seabed, even though finer sands can reach higher levels in the water column than coarser sand.

At the mouth during high river discharge conditions, the mud export at the surface is more intense than during low discharge conditions (Figure 11a and 12 a). It develops the turbid plume further seaward (Figure 19 in supplementary data) and transports more mud toward the subtidal mud patch on the continental shelf. However, the mud import at the bottom is also more intense due to the enhanced baroclinic circulation (Figures 11b and 12b). It induces a large mud transport from the mouth area toward the estuary. Due to larger mud concentrations at the bottom, the import wins against the export, resulting in larger up-estuary residual (i.e., depth-averaged) mud fluxes at the mouth for high river discharge conditions. These considerations and the enhanced baroclinic circulation can also be seen clearly in Figure 13 (and Figure 21, supplementary material), with strong up-estuary currents close to the bottom and seaward velocities near the surface.

On the other hand, the different behavior could be explained by looking further into the difference in critical shear stresses for each class. Associated with the tidal asymmetry (between ebb and flood) and the modulation by neap and spring tides, the residual transport of each class can be different. Such asymmetrical dynamics between neap and spring tides have been shown previously by Diaz et al. (2020) in this same area, using the same model. The enhanced baroclinic circulation during high river flow and the asymmetrical dynamics between neap and spring are also shown as vertical profiles of longitudinal current velocity and salinity in Figure 20, supplementary material. In the case where the critical shear stress is not reached during one of the tidal phases for instance, or if the time during which the threshold is exceeded is asymmetrical between the different phases of the tide, these neap/spring asymmetries most probably induce opposite dominant transport directions at these time scales. Moreover, as can be seen in Figure 13, the residual velocities during high and low river discharges are quite different at the section Verdon. The velocity magnitude is higher during high river flow conditions, which ultimately drives stronger sediment fluxes but could also potentially bring in suspension coarser sediment classes that wouldn't be transported during low river discharge conditions. Besides, Figure 13 also shows strong horizontal velocity gradients which most probably play an important role in driving different transport behaviors between the sediment classes, as the nature of both the locally available sediment mass on the seabed and the suspended particles is possibly different between the left and the right bank.

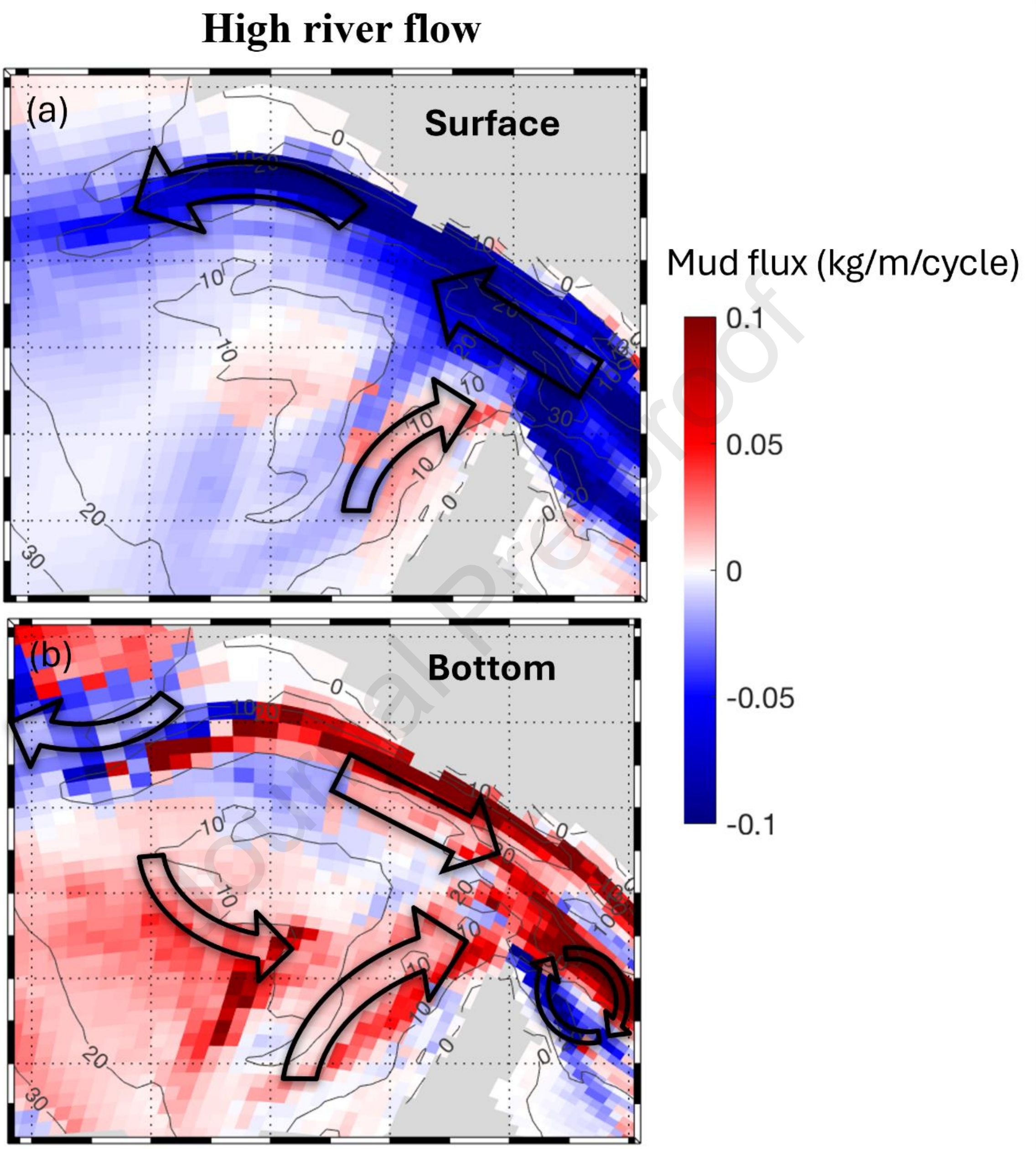

Figure 11 (a) Surface and (b) bottom residual fluxes of mud over a neap-spring cycle during high river flow (February - march 2016) (red is directed towards the estuary, blue is directed offshore). Gray lines represent the isobaths.

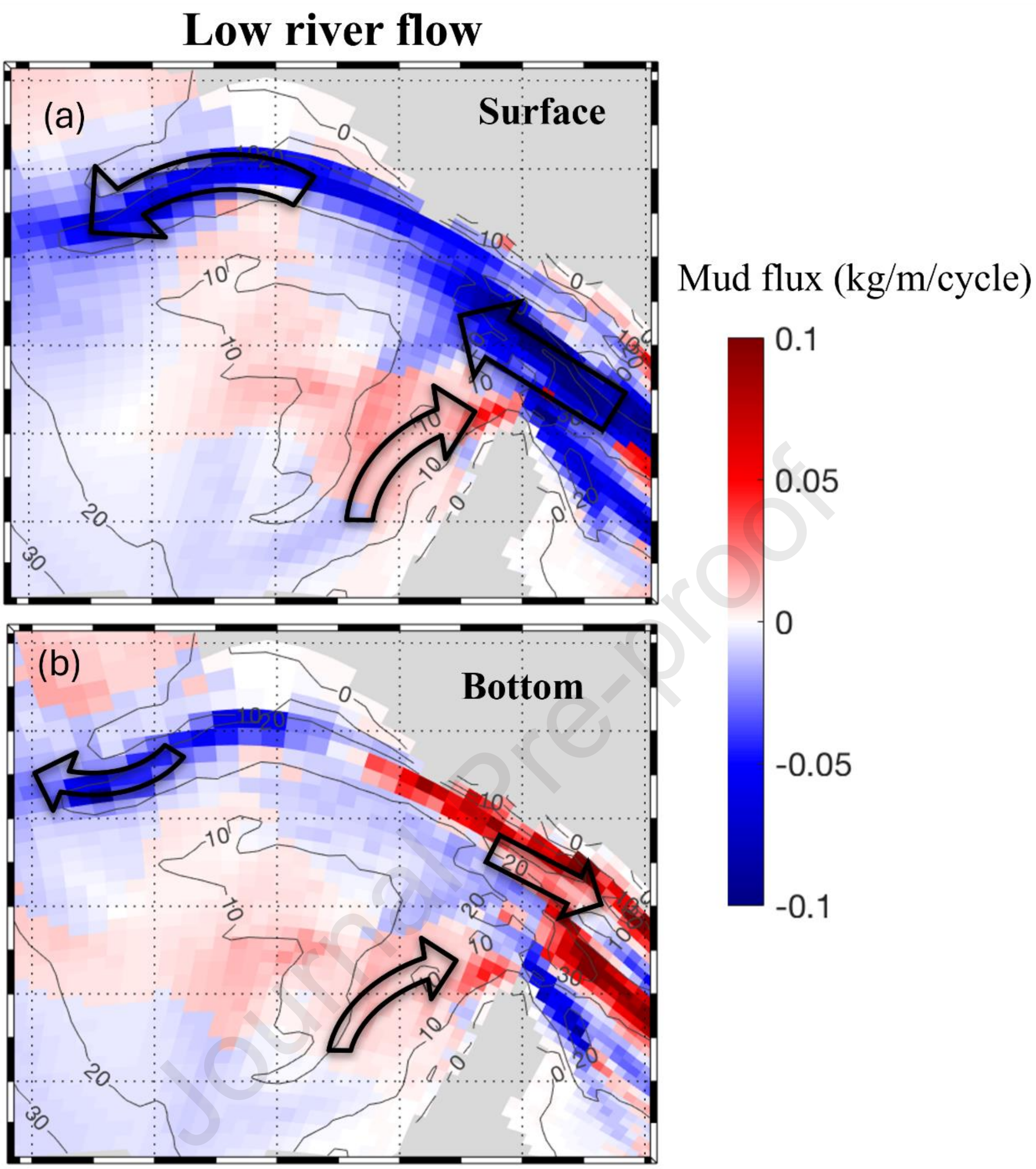

Figure 12 (a) Surface and (b) bottom residual fluxes of mud over a neap-spring cycle during low river flow (August - September 2016) (red is directed towards the estuary, blue is directed offshore). Gray lines represent the isobaths.

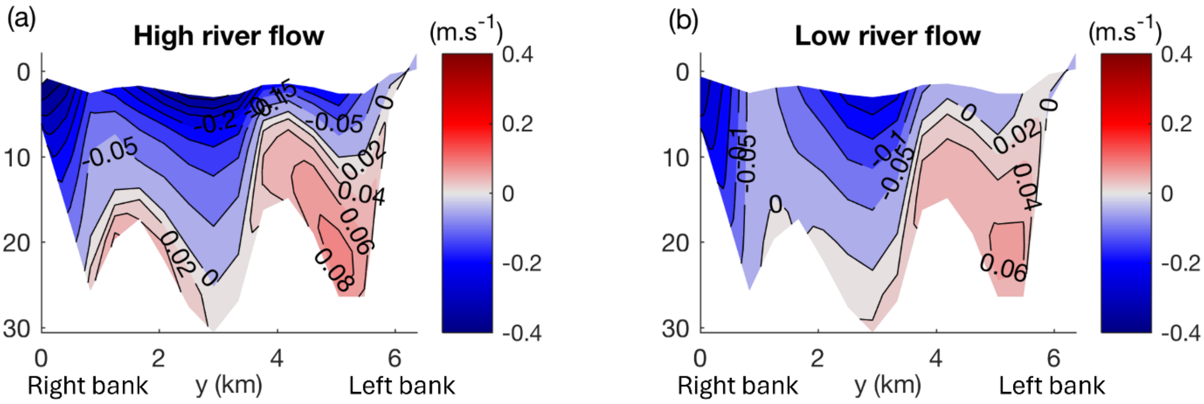

Figure 13 Residual velocities at the estuarine mouth through the Verdon section (positive up-estuary, vertical reference: mean sea level). Average over a neap/spring cycle during periods of (a) high river flow and (b) low river flow.

Based on the model results, the residual sediment flux (all sediment classes together) averaged over the two simulated years is estimated at approximately -0.47 Mt/yr upstream the mouth (through the Verdon section, negative fluxes are directed offshore) and approximately -1 Mt/yr at the 25m-isobath. Given the uncertainties estimated by Diaz et al. (2020), there is a residual export of mud (from the estuary towards the mouth) of 2.85 ± 2.65 Mt/yr and a residual import of sand and gravel into the estuary of 2.4 ± 1.2 Mt/yr through the Verdon section. The behavior is different between the two simulated years: at the upstream estuarine mouth (Verdon section), there is a residual import of sediment toward the estuary of about 0.2 Mt/yr under wet conditions in 2016 and residual export of sediment offshore of about 1.1 Mt/yr during the next dryer year.

Similar contrasting behavior between different yearly hydrological conditions have recently been assessed by Schulz et al. (2018) in the Seine Estuary. This is the consequence of an intensified baroclinic circulation during wetter conditions which enhanced up-estuary transport. The impact of such a density-induced residual circulation on both mud and sand dynamics might be often neglected or underestimated even though it has already been proven of prime importance. It was assessed for instance by Pandoe & Edge (2004) who simulated very different suspended sediment dynamics in response to barotropic and baroclinic modes in the case of an idealized tidal inlet in stratified water. Burchard et al. (2008) also identified the horizontal density differences between the Wadden Sea waters and the North Sea to be the driving force for suspended matter transport and fine sediment accumulation in the Wadden Sea. Moreover, similarly to what occurred in this work, Gelfenbaum et al. (2017) found that accounting for the density stratification tends to significantly reduce the export of sands at the mouth of the Columbia River toward the Pacific ocean.

5.3 Dynamics of a shelf mud patch

One of the main achievements of this study in terms of sedimentary features, is the simulation of a subtidal mudflat on a mostly sandy continental shelf in a mud accumulation area located to the North-West of the estuarine mouth and to the East of the currently active WGMP, around 30-40 m water depth. In this area, the particles settle down from concentrated turbid waters coming from the estuary, brought specifically to this confined region by tidal currents, combined with less energetic wave action due to the depth promoting fine particles deposition (compared to nearer the coast (Lamarque et al., 2021)).

The slight difference in location between the observed and simulated mud accumulation areas can be explained by several reasons. First, the geological interpretation of the formation of the WGMP is that estuarine mud started to accumulate offshore by 2000 years BP when the estuarine accommodation space was filled (Lesueur et al., 2002). The prevailing environmental conditions in that period, and especially the mud export rate from the estuary cannot be fully considered in the model, based on a present-day setup. Second, the initial bed composition in the model was uniform over the whole domain. However, it is known that the WGMP is a consolidated muddy patch surrounded by a sandy bed and, because of this state of consolidation, the sediment is more difficult to erode on this particular mud patch compared to the surroundings (Barthe & Castaing, 1989). Moreover, the theoretical analysis of Barthe & Castaing (1989) on the bed shear stress required to mobilize the sediments on the shelf showed that a typical swell of 12 s period and 2 m significant wave height would be enough to mobilize loose sediments on the shelf (conditions occurring on average 90 days per year) while waves of 6 to 10 meters would be necessary to rework consolidated mud from the WGMP (happening on average only 6 days per year). Thus, even if the consolidation process is reproduced by the model, fresh mud deposited around 30 m depth as simulated by the model is likely to be resuspended quite easily. Then, taking into account a consolidated muddy bed between 30 and 70 m water depth over the WGMP from the beginning of the simulation would prevent the sediments deposited there to be reworked. It also has to be noted that trawling effect was not taken into account. Yet, it was shown in previous studies to have a huge impact in this area (Mengual et al., 2016; Lamarque et al., 2021) and it could potentially influence the location and development of the mud patch, even though it is of less influence than the local hydrodynamics. Finally, the initial formation of the mud patch resulted from the infilling of a depressed area on the continental shelf which is not represented by the modern bathymetry in the model. However, the fact that the model still reproduced an accumulation of mud in the vicinity of the observed mud patch indicates that local hydrodynamics alone already induced the formation of a mud patch from the deposit of mud particles coming from the estuary.

The results of this study assessed that the trapping efficiency of the subtidal mudflat decreases with increasing wave-induced shear stress (Figure 14). The deposition is enhanced (and the erosion is reduced) during high river discharge compared to lower river flow conditions, not because the wave action on sediment resuspension is reduced, but because, during high river flow, the estuarine turbid plume is more concentrated and spreads further offshore (see Figure 19 in supplementary data as well as Constantin et al. (2018) and Froidefond et al. (1998) for instance). It demonstrates the primordial effects of wave action, hydrological regime and riverine sediment supply to the dynamics of such subtidal muddy structures, which can be reliably extrapolated to similar shelf muddy deposits such as the New England Mud Patch (Bothner et al., 1981; Goff et al., 2019) or the Nantucket Shoals Mud Patch (Dalyander et al., 2013).

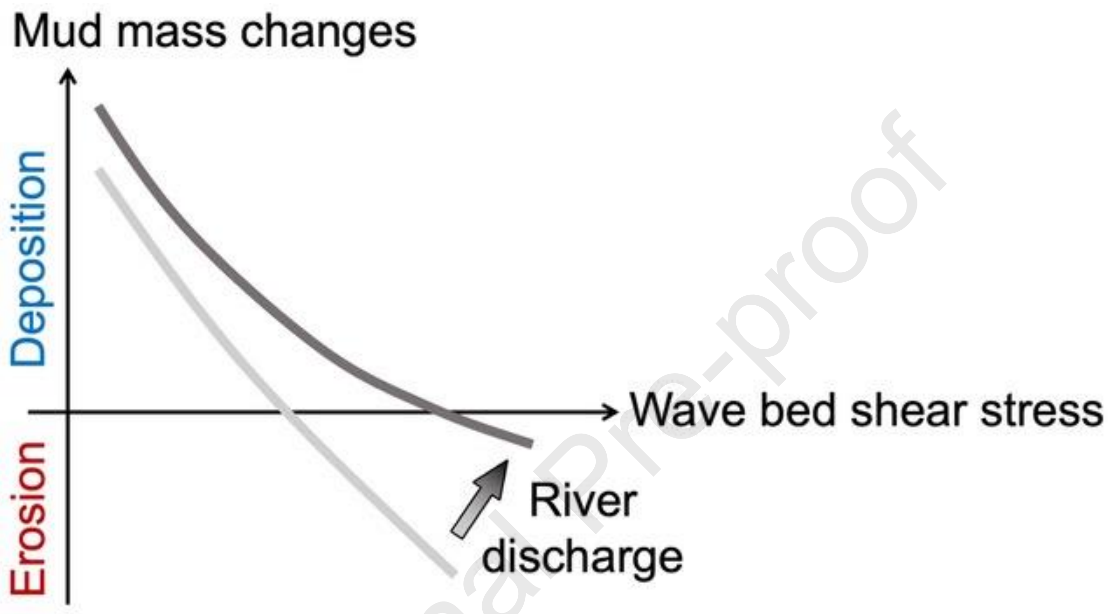

Figure 14 Scheme of the functioning of the mudflat deposition and erosion processes with regards to local hydrodynamics

Jouanneau et al. (1989), followed by Lesueur et al. (2002) and Lamarque et al. (2021), found that the main deposits in this area are alternating sandy sediment strata, presumably deposited during storms, and muddy laminated layers accumulated during large flood events, which are likely to be eroded easily during the following energetic events and to feed the distal part of the mud patch. This corroborates the functioning reproduced by the model and could help explain further the differences between the simulated and observed mudflat locations: the time scales represented here could be too short to reproduce the long-term dynamics of sediment reworking towards the deeper part of the WGMP. On the other hand, the simulated sedimentation rates of about 4 cm/yr over the simulated mud accumulation area are largely overestimated: Lesueur et al. (2001) and more recently Dubosq et al. (2021) using radionuclide analysis calculated rates of about 0.1 cm/yr in this inner area as well as in the deepest part of the WGMP, while up to 0.4 cm/yr of mud are accumulating around 45-50 m water depth. The model results in terms of seabed sediment accumulation (mass and thickness) should thus be considered carefully. However, the suspended sediment dynamics and, as such, the impact of hydrodynamics on sediment accumulation or dispersion remains a validated and trustworthy information given by the model.

Such behavior raises the issue of the fate of muddy structures facing climate change and anthropogenic activities. Several studies have stressed the expected consequences of human disturbances on the riverine sediment supply to continental shelves in the coming decades, such as the increase in river damming (Besset et al., 2019; Ouillon, 2018; Vörösmarty et al., 2003; Yang et al., 2011). The amount of fluvial material retained by reservoirs and dams is estimated at 25-30% on average around the globe but can go up to 95% locally in the Nile and Ebro rivers for example (Besset et al., 2019; Vörösmarty et al., 2003). Given the contribution of river discharge to the mudflat accumulation rate highlighted in this study, this suggests a possible shrinkage of muddy deposited areas under decreasing supplied material from the rivers. One can also wonder what the impact of sea level rise is expected to be. Van Maanen et al. (2018) studied the expected consequences on the estuarine circulation and the estuarine turbidity maximum dynamics. They found that, with sea level rise, in the estuary, the stratification seems to be enhanced downstream and thus, the gravitational circulation as well. Upstream, there is an increase of the tidal range and associated tidal current. However, these consequences are found to be of minor importance compared to the impacts of variations in river discharge. River discharge has been decreasing over the past decades and is expected to keep decreasing in the future. This is expected to increase the upstream migration of both the salinity front and the ETM. From what has been seen in the present study, on top of the consequences of river damming, this could further decrease the amount of particles exported at the estuarine mouth and the supply of particles to the subtidal mudflat.

Another aspect of climate change that questions the fate of these structures relates to the impact on storminess, and as such, wave action. Even though no significant trend has been evidenced on a global scale over the 20th century (Houghton, 2001), Graham & Diaz (2001) identified an increase in the intensity of winter cyclones in the North Pacific Ocean. More recently, Bhatia et al. (2019) also found a clear tendency to an increase in tropical cyclone intensities in the Atlantic basin. The intensification of offshore storm activities results in a much stronger wave regime along the coasts of both the American and the European continents (Bromirski et al., 2003; Lozano et al., 2004). Such an increase in the expected wave regime on continental shelves is likely to impact the functioning of muddy deposits by increasing sediment resuspension and preventing particles to settle down in these areas. Thus, two primordial factors driving sediment accumulation on shelf mud patches highlighted in this work, are expected to be strongly modified in the future, in a sense that could severely impact the functioning and volume of these structures. An example of such devastating consequences has been documented by Ai-jun et al. (2020) in the Minjiang River of Southern China, where the intensification of damming affected the accumulation rate of fines in the subaqueous delta and altered its functioning.

Another interesting point of such a method based on numerical modeling lies in the richness of information that the model can provide. In this work, it was chosen to distinguish different sources of sediment, which showed that 26% of the mud accumulated on the mudflat during two years originates from the estuary. Being able to evaluate the contribution of different sources is of prime interest to assess the impact of terrigenous contaminants or to predict the fate of muddy structures facing strong riverine sediment retention. Moreover, in the case of shelf mud patches where the main sediment sourcing remains unidentified such as the New England Mud Patch (Goff et al., 2019), such numerical experiments could help trace back the particle origins.

6. Conclusions

The sediment transfers between a major macrotidal estuary of Western Europe (the Gironde Estuary) and its adjacent continental shelf were investigated and quantified through a thoroughly calibrated and validated three-dimensional mixed-sediment (mud, sand, and gravel) transport numerical model. Multi-year simulations driven by realistic forcing were carried out to ensure sediment model stability and to account for contrasted hydro- and meteorological conditions. The objectives of this work were twofold: to investigate the impact of the hydro-meteorological conditions on (i) the sediment fluxes at the mouth and (ii) the sediment dynamics of accumulation areas on the adjacent continental shelf, and especially of shelf subtidal mudflats.

After seven years of simulation, this model reasonably well reproduced the observed sediment dynamics at four different locations: two stations were located in the upper and central estuary, and two other measurement stations were deployed offshore the estuarine mouth: at 20-m water depth at the outlet of the estuarine channel and at 40-m water depth, on a well-known subtidal mudflat (the West Gironde Mud Patch). Despite an underestimation of the sediment concentration in the ETM area, the estuarine seasonal dynamics associated with river discharge (*i.e.* the ETM longitudinal migration) were satisfactorily reproduced by the model. Moreover, on the adjacent continental shelf, the sediment dynamics were in very good agreement with the observed tendencies associated with wave action which is the dominant mechanism driving sediment resuspension in this area.

The residual sediment fluxes between the estuary and the ocean exhibited large discrepancies between the different sediment classes. On average over the two simulated years, there is a residual export of mud and fine sand toward the open ocean through the 25m-isobath and a residual import of very fine and medium sand toward the estuarine mouth. Large discrepancies are revealed by the model for contrasted hydro- and meteorological conditions as well. During wet conditions, the reinforced density gradients drive strong baroclinic circulation which tends to dominate the sediment dynamics over the barotropic export of mud particles, contrarily to what might sometimes be believed.

The model reproduced the signature of a subtidal mud accumulation area over the continental shelf around 30-40 m water depth, located to the North-East of the current active part of the West Gironde Mud Patch. On average over the two simulated years, 26% of the mud mass accumulated on this area comes from the estuary. The trapping efficiency of the mudflat is negatively correlated with wave action. The mud mostly accumulates in this area for wave-induced bed shear stresses lower than 0.3 N/m^2. Moreover, due to the estuarine turbid plume being more concentrated and developed during winter, the trapping efficiency of the mud body is enhanced compared to lower discharges. It demonstrates the primordial effects of both wave action and riverine sediment supply to the dynamics of such subtidal muddy structures, which raises concern about their fate facing climate change and human disturbances (*i.e.* potential changes in liquid and solid riverine supplies, as well as wave conditions).

Data Availability

Numerical simulations related to this study along with a 10-year hindcast using the model presented here can be found here: https://doi.org/10.12770/44ac4d72-c606-42ba-bf22-89e6520e0894 (Diaz et al., 2023). The GEMMES dataset (Grasso et al., 2021) was collected in the framework of the METEOR 2017 cruises and is available at https://www.seanoe.org/data/00678/78968/.

Acknowledgments

We would like to thank David Le Berre and Benedicte Thouvenin for their help with the fieldwork and the model configuration, respectively.

Funding

This work was primarily initiated as part of the AMORAD project and received a state fund managed by the French National Research Agency (ANR) in the frame of the Investments for the future Program (AMORAD-ANR-11-RSNR-0002). This work was also supported by the MAGMA project cofounded by the COTE Cluster of Excellence (ANR-10-LABX-45) and the French Biodiversity Agency.

References

Ai-jun, W., Xiang, Y., Zhen-kun, L., Liang, W., & Jing, L. (2020). Response of sedimentation processes in the Minjiang River subaqueous delta to anthropogenic activities in the river basin. *Estuarine, Coastal and Shelf Science*, *232*, 106484. https://doi.org/10.1016/j.ecss.2019.106484

Alahmed, S., Ross, L., & Sottolichio, A. (2021). The role of advection and density gradients in driving the residual circulation along a macrotidal and convergent estuary with non-idealized geometry. *Continental Shelf Research*, *212*, 104295. https://doi.org/10.1016/j.csr.2020.104295

Allen, G. P., Salomon, J. C., Bassoullet, P., Du Penhoat, Y., & de Grandpré, C. (1980). Effects of tides on mixing and suspended sediment transport in macrotidal estuaries. *Sedimentary Geology*, *26*(1), 69–90. https://doi.org/10.1016/0037-0738(80)90006-8

Azaroff, A., Miossec, C., Lanceleur, L., Guyoneaud, R., & Monperrus, M. (2020). Priority and emerging micropollutants distribution from coastal to continental slope sediments: A case study of Capbreton Submarine Canyon (North Atlantic Ocean). *Science of The Total Environment*, *703*, 135057. https://doi.org/10.1016/j.scitotenv.2019.135057

Barthe, X., & Castaing, P. (1989). Etude théorique de l'action des courants de marée et des houles sur les sédiments du plateau continental du Golfe de Gascogne. *Oceanologica Acta*, *12*(4), 325–334.

Bassetti, M.-A., Berné, S., Sicre, M.-A., Dennielou, B., Alonso, Y., Buscail, R., Jalali, B., Hebert, B., & Menniti, C. (2016). Holocene hydrological changes in the Rhône River (NW Mediterranean) as recorded in the marine mud belt. *Climate of the Past Discussions*, *12*(7), 1539. https://doi.org/10.5194/cp-12-1539-2016

Besset, M., Anthony, E. J., & Bouchette, F. (2019). Multi-decadal variations in delta shorelines and their relationship to river sediment supply: An assessment and review. *Earth-Science Reviews*, *193*, 199–219. https://doi.org/10.1016/j.earscirev.2019.04.018

Beven, K. (1993). Prophecy, reality and uncertainty in distributed hydrological modelling. *Advances in Water Resources*, *16*(1), 41–51. https://doi.org/10.1016/0309-1708(93)90028-E

Bhatia, K. T., Vecchi, G. A., Knutson, T. R., Murakami, H., Kossin, J., Dixon, K. W., & Whitlock, C. E. (2019). Recent increases in tropical cyclone intensification rates. *Nature Communications*, *10*(1), 635. https://doi.org/10.1038/s41467-019-08471-z

Borgeld, J. C. (1987). *Holocene stratigraphy and sedimentation on the northern California continental shelf* [PhD Thesis].

Bothner, M. H., Spiker, E. C., Johnson, P. P., Rendigs, R. R., & Aruscavage, P. J. (1981). Geochemical evidence for modern sediment accumulation on the continental shelf off southern New England. *Journal of Sedimentary Research*, *51*(1), 281–292. https://doi.org/10.1306/212F7C70-2B24-11D7-8648000102C1865D

Bromirski, P. D., Flick, R. E., & Cayan, D. R. (2003). Storminess Variability along the California Coast: 1858–2000. *Journal of Climate*, *16*(6), 982–993. https://doi.org/10.1175/1520-0442(2003)016<0982:SVATCC>2.0.CO;2

Burchard, H., Flöser, G., Staneva, J. V., Badewien, T. H., & Riethmüller, R. (2008). Impact of Density Gradients on Net Sediment Transport into the Wadden Sea. *Journal of Physical Oceanography*, *38*(3), 566–587. https://doi.org/10.1175/2007JPO3796.1

Castaing, P., & Allen, G. P. (1981). Mechanisms controlling seaward escape of suspended sediment from the Gironde: A macrotidal estuary in France. *Marine Geology*, *40*(1), 101–118. https://doi.org/10.1016/0025-3227(81)90045-1

Castaing, P., & Jouanneau, J. M. (1987). Les apports sédimentaires actuels d'origine continentale aux océans. *Bulletin de l'Institut de Géologie Du Bassin d'Aquitaine*, *41*, 53–65.

Constantin, S., Doxaran, D., Derkacheva, A., Novoa, S., & Lavigne, H. (2018). Multi-temporal dynamics of suspended particulate matter in a macro-tidal river Plume (the Gironde) as observed by satellite data. *Estuarine, Coastal and Shelf Science*, *202*, 172–184. https://doi.org/10.1016/j.ecss.2018.01.004

Dalrymple, R. W., & Choi, K. (2007). Morphologic and facies trends through the fluvial–marine transition in tide-dominated depositional systems: A schematic framework for environmental and sequence-stratigraphic interpretation. *Earth-Science Reviews*, *81*(3), 135–174. https://doi.org/10.1016/j.earscirev.2006.10.002

Dalyander, P. S., Butman, B., Sherwood, C. R., Signell, R. P., & Wilkin, J. L. (2013). Characterizing wave- and current- induced bottom shear stress: U.S. middle Atlantic continental shelf. *Continental Shelf Research*, *52*, 73–86. https://doi.org/10.1016/j.csr.2012.10.012

de Mahiques, M. M., Figueira, R. C. L., Sousa, S. H. de M., Santos, R. F. dos, Ferreira, P. A. de L., Kim, B. S. M., Cazzoli y Goya, S., de Matos, M. C. S. N., & Bícego, M. C. (2020). Sedimentation on the southern Brazilian shelf mud depocenters: Insights on potential source areas. *Journal of South American Earth Sciences*, *100*, 102577. https://doi.org/10.1016/j.jsames.2020.102577

de Mahiques, M. M., Hanebuth, T. J. J., Martins, C. C., Montoya-Montes, I., Alcántara-Carrió, J., Figueira, R. C. L., & Bícego, M. C. (2016). Mud depocentres on the continental shelf: A neglected sink for anthropogenic contaminants from the coastal zone. *Environmental Earth Sciences*, *75*(1), 44. https://doi.org/10.1007/s12665-015-4782-z

Dias, J. M. A., Jouanneau, J. M., Gonzalez, R., Araújo, M. F., Drago, T., Garcia, C., Oliveira, A., Rodrigues, A., Vitorino, J., & Weber, O. (2002). Present day sedimentary processes on the northern Iberian shelf. *Progress in Oceanography*, *52*(2), 249–259. https://doi.org/10.1016/S0079-6611(02)00009-5

Diaz, M. (2019). *Modélisation numérique des transferts sédimentaires de l'estuaire de la Gironde au plateau continental* [These de doctorat, Brest]. http://www.theses.fr/2019BRES0095

Diaz, M., Grasso, F., & Caillaud, M. (2023). *CurviGironde Hindcast* [Dataset]. IFREMER. https://doi.org/10.12770/44ac4d72-c606-42ba-bf22-89e6520e0894

Diaz, M., Grasso, F., Hir, P. L., Sottolichio, A., Caillaud, M., & Thouvenin, B. (2020). Modeling Mud and Sand Transfers Between a Macrotidal Estuary and the Continental Shelf: Influence of the Sediment Transport Parameterization. *Journal of Geophysical Research: Oceans*, *125*(4), e2019JC015643. https://doi.org/10.1029/2019JC015643

Dubosq, N., Schmidt, S., Walsh, J. P., Grémare, A., Gillet, H., Lebleu, P., Poirier, D., Perello, M.-C., Lamarque, B., & Deflandre, B. (2021). A first assessment of organic carbon burial in the West Gironde

Mud Patch (Bay of Biscay). *Continental Shelf Research*, *221*, 104419. https://doi.org/10.1016/j.csr.2021.104419

Dunn, R. J. K., Zigic, S., Burling, M., & Lin, H.-H. (2015). Hydrodynamic and Sediment Modelling within a Macro Tidal Estuary: Port Curtis Estuary, Australia. *Journal of Marine Science and Engineering*, *3*(3), 720–744. https://doi.org/10.3390/jmse3030720

Eckles, B. J., Fassell, M. L., & Anderson, J. B. (2004). Late Quaternary evolution of the wave/storm-dominated Central Texas Shelf. In *Late Quaternary evolution of the Northern Gulf of Mexico* (Vol. 79, pp. 271–287). https://doi.org/10.2110/pec.04.79.0271

Etcheber, H., Schmidt, S., Sottolichio, A., Maneux, E., Chabaux, G., Escalier, J.-M., Wennekes, H., Derriennic, H., Schmeltz, M., Quéméner, L., Repecaud, M., Woerther, P., & Castaing, P. (2011). Monitoring water quality in estuarine environments: Lessons from the MAGEST monitoring program in the Gironde fluvial-estuarine system. *Hydrol. Earth Syst. Sci.*, *15*(3), 831–840. https://doi.org/10.5194/hess-15-831-2011

Froidefond, J.-M., Jegou, A.-M., Hermida, J., Lazure, P., & Castaing, P. (1998). Variabilité du panache turbide de la Gironde par télédétection. Effets des facteurs climatiques. *Oceanologica Acta*, *21*(2), Article 2. https://doi.org/10.1016/S0399-1784(98)80008-X

Gao, S., & Collins, M. B. (2014). Holocene sedimentary systems on continental shelves. *Marine Geology*, *352*, 268–294. https://doi.org/10.1016/j.margeo.2014.03.021

Garcia, J., Mojtahid, M., Howa, H., Michel, E., Schiebel, R., Charbonnier, C., Anschutz, P., & Jorissen, F. J. (2013). Benthic and Planktic Foraminifera as Indicators of Late Glacial to Holocene Paleoclimatic Changes in a Marginal Environment: An Example from the Southeastern Bay of Biscay. *Acta Protozoologica*, *52*(3). http://psjd.icm.edu.pl/psjd/element/bwmeta1.element.ojs-issn-1689-0027-year-2013-volume-52-issue-3-article-4075

Garnaud, S., Lesueur, P., Clet, M., Lesourd, S., Garlan, T., Lafite, R., & Brun-Cottan, J.-C. (2003). Holocene to modern fine-grained sedimentation on a macrotidal shoreface-to-inner-shelf setting (eastern Bay of the Seine, France). *Marine Geology*, *202*(1), 33–54. https://doi.org/10.1016/S0025-3227(03)00266-4

Gelfenbaum, G., Elias, E., & Stevens, A. W. (2017). Investigation of input reduction techniques for morphodynamic modeling of complex inlets with baroclinic forcing. *Coastal Dynamics 2017*, 1142–1154.

Gillet, H., & Deflandre, B. (2018). *JERICOBENT-5-TH cruise,Thalia R/V*. https://doi.org/10.17600/18000425

Goff, J. A., Reed, A. H., Gawarkiewicz, G., Wilson, P. S., & Knobles, D. P. (2019). Stratigraphic analysis of a sediment pond within the New England Mud Patch: New constraints from high-resolution chirp acoustic reflection data. *Marine Geology*, *412*, 81–94. https://doi.org/10.1016/j.margeo.2019.03.010

Gonzalez, R., Araújo, M. F., Burdloff, D., Cachão, M., Cascalho, J., Corredeira, C., Dias, J. M. A., Fradique, C., Ferreira, J., Gomes, C., Machado, A., Mendes, I., & Rocha, F. (2007). Sediment and pollutant transport in the Northern Gulf of Cadiz: A multi-proxy approach. *Journal of Marine Systems*, *68*(1–2), 1–23. https://doi.org/10.1016/j.jmarsys.2006.10.007

Graham, N. E., & Diaz, H. F. (2001). Evidence for Intensification of North Pacific Winter Cyclones since 1948. *Bulletin of the American Meteorological Society*, *82*(9), 1869–1894. https://doi.org/10.1175/1520-0477(2001)082<1869:EFIONP>2.3.CO;2

Grasso, F. (2017). *METEOR 2017 cruise,Côtes De La Manche R/V*. https://doi.org/10.17600/17010200

Grasso, F., Bocher, A., Jacquet, M., Le Berre, D., & Lecornu, F. (2021). *Gironde Estuary Mouth MEasurement Stations (GEMMES)*. SEANOE. https://doi.org/10.17882/78968

Grasso, F., Le Hir, P., & Bassoullet, P. (2015). Numerical modelling of mixed-sediment consolidation. *Ocean Dynamics*, *65*(4), 607–616. https://doi.org/10.1007/s10236-015-0818-x

Grasso, F., Verney, R., Le Hir, P., Thouvenin, B., Schulz, E., Kervella, Y., Khojasteh Pour Fard, I., Lemoine, J.-P., Dumas, F., & Garnier, V. (2018). Suspended Sediment Dynamics in the Macrotidal Seine Estuary (France): 1. Numerical Modeling of Turbidity Maximum Dynamics. *Journal of Geophysical Research: Oceans*, *123*(1), 558–577. https://doi.org/10.1002/2017JC013185

Hanebuth, T. J. J., Lantzsch, H., & Nizou, J. (2015). Mud depocenters on continental shelves—Appearance, initiation times, and growth dynamics. *Geo-Mar Lett*, *35*(6), 487–503. https://doi.org/10.1007/s00367-015-0422-6

Houghton, J. T. (2001). *Climate Change 2001: The Scientific Basis*.

Jalón-Rojas, I., Schmidt, S., & Sottolichio, A. (2015). Turbidity in the fluvial Gironde Estuary (southwest France) based on 10-year continuous monitoring: Sensitivity to hydrological conditions. *Hydrology and Earth System Sciences*, *19*(6), 2805.

Jay, D. A., Uncles, R. J., Largeir, J., Geyer, W. R., Vallino, J., & Boynton, W. R. (1997). A review of recent developments in estuarine scalar flux estimation. *Estuaries*, *20*(2), 262–280. https://doi.org/10.2307/1352342

Jolliff, J. K., Kindle, J. C., Shulman, I., Penta, B., Friedrichs, M. A. M., Helber, R., & Arnone, R. A. (2009). Summary diagrams for coupled hydrodynamic-ecosystem model skill assessment. *Journal of Marine Systems*, *76*(1), 64–82. https://doi.org/10.1016/j.jmarsys.2008.05.014

Jouanneau, J. M., Weber, O., Cremer, M., & Castaing, P. (1999). Fine-grained sediment budget on the continental margin of the Bay of Biscay. *Deep Sea Research Part II: Topical Studies in Oceanography*, *46*(10), 2205–2220. https://doi.org/10.1016/S0967-0645(99)00060-0

Jouanneau, J. M., Weber, O., Latouche, C., Vernet, J. P., & Dominik, J. (1989). Erosion, non-deposition and sedimentary processes through a sedimentological and radioisotopic study of surficial deposits from the "Ouest-Gironde vasière" (Bay of Biscay). *Continental Shelf Research*, *9*(4), 325–342. https://doi.org/10.1016/0278-4343(89)90037-X

Jouanneau, J.-M., & Latouche, C. (1981). *The gironde estuary*. https://www.schweizerbart.de/publications/detail/isbn/9783510570102

Krone, R. B. (1962). Flume studies of transport of sediment in estrarial shoaling processes. *Final Report, Hydr. Engr. and Samitary Engr. Res. Lab., Univ. of California*.

Lamarque, B., Deflandre, B., Galindo Dalto, A., Schmidt, S., Romero-Ramirez, A., Garabetian, F., Dubosq, N., Diaz, M., Grasso, F., Sottolichio, A., Bernard, G., Gillet, H., Cordier, M.-A., Poirier, D., Lebleu, P., Derriennic, H., Danilo, M., Murilo Barboza Tenório, M., & Grémare, A. (2021). Spatial

Distributions of Surface Sedimentary Organics and Sediment Profile Image Characteristics in a High-Energy Temperate Marine RiOMar: The West Gironde Mud Patch. *Journal of Marine Science and Engineering*, *9*(3), 242. https://doi.org/10.3390/jmse9030242

Lamarque, B., Deflandre, B., Schmidt, S., Bernard, G., Dubosq, N., Diaz, M., Lavesque, N., Garabetian, F., Grasso, F., Sottolichio, A., Rigaud, S., Romero-Ramirez, A., Cordier, M.-A., Poirier, D., Danilo, M., & Grémare, A. (2022). Spatiotemporal dynamics of surface sediment characteristics and benthic macrofauna compositions in a temperate high-energy River-dominated Ocean Margin. *Continental Shelf Research*, *247*, 104833. https://doi.org/10.1016/j.csr.2022.104833

Latouche, C., Jouanneau, J. M., Lapaquellerie, Y., Maillet, N., & Weber, O. (1991). Repartition des mineraux argileux sur le plateau continental Sud-Gascogne. *Oceanologica Acta, Special issue*. https://archimer.ifremer.fr/doc/00268/37889/

Lazure, P., & Dumas, F. (2008). An external–internal mode coupling for a 3D hydrodynamical model for applications at regional scale (MARS). *Advances in Water Resources*, *31*(2), 233–250. https://doi.org/10.1016/j.advwatres.2007.06.010

Le Hir, P., Cann, P., Waeles, B., Jestin, H., & Bassoullet, P. (2008). Chapter 11 Erodibility of natural sediments: Experiments on sand/mud mixtures from laboratory and field erosion tests. In T. Kusuda, H. Yamanishi, J. Spearman, & J. Z. Gailani (Eds.), *Proceedings in Marine Science* (Vol. 9, pp. 137–153). Elsevier. https://doi.org/10.1016/S1568-2692(08)80013-7

Le Hir, P., Cayocca, F., & Waeles, B. (2011). Dynamics of sand and mud mixtures: A multiprocess-based modelling strategy. *Continental Shelf Research*, *31*(10, Supplement), S135–S149. https://doi.org/10.1016/j.csr.2010.12.009

Lesueur, P., Jouanneau, J.-M., Boust, D., Tastet, J.-P., & Weber, O. (2001). Sedimentation rates and fluxes in the continental shelf mud fields in the Bay of Biscay (France). *Continental Shelf Research*, *21*(13), 1383–1401. https://doi.org/10.1016/S0278-4343(01)00004-8

Lesueur, P., Tastet, J. P., & Weber, O. (2002). Origin and morphosedimentary evolution of fine-grained modern continental shelf deposits: The Gironde mud fields (Bay of Biscay, France). *Sedimentology*, *49*(6), 1299–1320. https://doi.org/10.1046/j.1365-3091.2002.00498.x

Li, Z. H., Nguyen, K. D., Bruncottan, J. C., & Martin, J. M. (1994). Numerical-simulation of the turbidity maximum transport in the Gironde estuary (France). *Oceanologica Acta*, *17*(5), 479–500.

Liu, S., Shi, X., Liu, Y., Zhu, Z., Yang, G., Zhu, A., & Gao, J. (2011). Concentration distribution and assessment of heavy metals in sediments of mud area from inner continental shelf of the East China Sea. *Environmental Earth Sciences*, *64*(2), 567–579. https://doi.org/10.1007/s12665-011-0941-z

Lozano, I., Devoy, R. J. N., May, W., & Andersen, U. (2004). Storminess and vulnerability along the Atlantic coastlines of Europe: Analysis of storm records and of a greenhouse gases induced climate scenario. *Marine Geology*, *210*(1), 205–225. https://doi.org/10.1016/j.margeo.2004.05.026

McCave, I. N. (1972). Transport and escape of fine-grained sediment from shelf areas. *Shelf Sediment Transport: Process and Pattern*, 225–248.

Mengual, B., Cayocca, F., Le Hir, P., Draye, R., Laffargue, P., Vincent, B., & Garlan, T. (2016). Influence of bottom trawling on sediment resuspension in the 'Grande-Vasière' area (Bay of Biscay, France). *Ocean Dynamics*, *66*(9), 1181–1207. https://doi.org/10.1007/s10236-016-0974-7

Mengual, B., Hir, P. L., Cayocca, F., & Garlan, T. (2017). Modelling Fine Sediment Dynamics: Towards a Common Erosion Law for Fine Sand, Mud and Mixtures. *Water*, *9*(8), 564. https://doi.org/10.3390/w9080564

Mojtahid, M., Durand, M., Coste, P.-O., Toucanne, S., Howa, H., Nizou, J., Eynaud, F., & Penaud, A. (2019). Millennial-scale Holocene hydrological changes in the northeast Atlantic: New insights from 'La Grande Vasière' mid-shelf mud belt. *The Holocene*, *29*(3), 467–480. https://doi.org/10.1177/0959683618816478

Nittrouer, C. A., Austin, J. A., Field, M. E., Kravitz, J. H., Syvitski, J. P. M., & Wiberg, P. L. (2007). Writing a Rosetta Stone: Insights into Continental-Margin Sedimentary Processes and Strata. In C. A. Nittrouer, J. A. Austin, M. E. Field, J. H. Kravitz, J. P. M. Syvitski, & P. L. Wiberg (Eds.), *Continental Margin Sedimentation* (pp. 1–48). Blackwell Publishing Ltd. https://doi.org/10.1002/9781444304398.ch1

Nittrouer, C. A., & Wright, L. D. (1994). Transport of particles across continental shelves. *Reviews of Geophysics*, *32*(1), 85–113. https://doi.org/10.1029/93RG02603

Nizou, J., Hanebuth, T. J. J., Heslop, D., Schwenk, T., Palamenghi, L., Stuut, J.-B., & Henrich, R. (2010). The Senegal River mud belt: A high-resolution archive of paleoclimatic change and coastal evolution. *Marine Geology*, *278*(1), 150–164. https://doi.org/10.1016/j.margeo.2010.10.002

Odum, E. P., & Barrett, G. W. (1971). *Fundamentals of ecology* (Vol. 3). Saunders Philadelphia.

Orseau, S., Huybrechts, N., Tassi, P., Pham Van Bang, D., & Klein, F. (2020). Two-dimensional modeling of fine sediment transport with mixed sediment and consolidation: Application to the Gironde Estuary, France. *International Journal of Sediment Research*. https://doi.org/10.1016/j.ijsrc.2019.12.005

Ouillon, S. (2018). Why and How Do We Study Sediment Transport? Focus on Coastal Zones and Ongoing Methods. *Water*, *10*(4), 390. https://doi.org/10.3390/w10040390

Palanques, A., Masqué, P., Puig, P., Sanchez-Cabeza, J. A., Frignani, M., & Alvisi, F. (2008). Anthropogenic trace metals in the sedimentary record of the Llobregat continental shelf and adjacent Foix Submarine Canyon (northwestern Mediterranean). *Marine Geology*, *248*(3–4), 213–227. https://doi.org/10.1016/j.margeo.2007.11.001

Palanques, A., Plana, F., & Maldonado, A. (1990). Recent influence of man on the Ebro margin sedimentation system, northwestern Mediterranean Sea. *Marine Geology*, *95*(3), 247–263. https://doi.org/10.1016/0025-3227(90)90119-5

Pandoe, W. W., & Edge, B. L. (2004). Cohesive sediment transport in the 3D-hydrodynamic-baroclinic circulation model,: Study case for idealized tidal inlet. *Ocean Engineering*, *31*(17), 2227–2252. https://doi.org/10.1016/j.oceaneng.2004.04.007

Partheniades, E. (1965). Erosion and deposition of cohesive soils. *Journal of the Hydraulics Division*, *91*(1), 105–139.

Porz, L., Zhang, W., Hanebuth, T. J. J., & Schrum, C. (2021). Physical processes controlling mud depocenter development on continental shelves – Geological, oceanographic, and modeling concepts. *Marine Geology*, *432*, 106402. https://doi.org/10.1016/j.margeo.2020.106402

Potter, P. E., Maynard, J. B., & Depetris, P. J. (2005). *Mud and Mudstones: Introduction and Overview*. Springer Science & Business Media.

Reise, R. (ed). (2001). *Ecological Comparisons of Sedimentary Shores*. Springer Science & Business Media.

Roland, A., & Ardhuin, F. (2014). On the developments of spectral wave models: Numerics and parameterizations for the coastal ocean. *Ocean Dynamics*, *64*(6), 833–846. https://doi.org/10.1007/s10236-014-0711-z

Schmidt, S., & Deflandre, B. (2018). *JERICOBENT-5 cruise,Côtes De La Manche R/V*. https://doi.org/10.17600/18000471

Schmidt, S., Etcheber, H., Sottolichio, A., & Castaing, P. (2016). Le réseau MAGEST: Bilan de 10 ans de suivi haute-fréquence de la qualité des eaux de l'estuaire de la Gironde. *Mesures Haute Résolution Dans l'environnement Marin Côtier. Presses Du CNRS*.

Schulz, E., Grasso, F., Hir, P. L., Verney, R., & Thouvenin, B. (2018). Suspended Sediment Dynamics in the Macrotidal Seine Estuary (France): 2. Numerical Modeling of Sediment Fluxes and Budgets Under Typical Hydrological and Meteorological Conditions. *Journal of Geophysical Research: Oceans*, *123*(1), 578–600. https://doi.org/10.1002/2016JC012638

Sommerfield, C. K., & Nittrouer, C. A. (1999). Modern accumulation rates and a sediment budget for the Eel shelf: A flood-dominated depositional environment. *Marine Geology*, *154*(1), 227–241. https://doi.org/10.1016/S0025-3227(98)00115-7

Sottolichio, A., Hir, P. L., & Castaing, P. (2000). Modeling mechanisms for the stability of the turbidity maximum in the Gironde estuary, France. In W. H. McAnally & A. J. Mehta (Eds.), *Proceedings in Marine Science* (Vol. 3, pp. 373–386). Elsevier. https://doi.org/10.1016/S1568-2692(00)80132-1

Soulsby, R. L. (1997). Dynamics of marine sands: A manual for practical applications. *Oceanographic Literature Review*, *9*(44), Article 44.

Swift, D. J. P., Stanley, D. J., & Curray, J. R. (1971). Relict Sediments on Continental Shelves: A Reconsideration. *The Journal of Geology*, *79*(3), 322–346. https://doi.org/10.1086/627629

Temmerman, S., Meire, P., Bouma, T. J., Herman, P. M. J., Ysebaert, T., & De Vriend, H. J. (2013). Ecosystem-based coastal defence in the face of global change. *Nature*, *504*(7478), 79–83. https://doi.org/10.1038/nature12859

Toublanc, F., Brenon, I., & Coulombier, T. (2016). Formation and structure of the turbidity maximum in the macrotidal Charente estuary (France): Influence of fluvial and tidal forcing. *Estuarine, Coastal and Shelf Science*, *169*, 1–14. https://doi.org/10.1016/j.ecss.2015.11.019

Van, L. A. (2012). *Modélisation du transport de sédiments mixtes sable-vase et application à la morphodynamique de l'estuaire de la Gironde (France)* [These de doctorat, Paris Est]. https://www.theses.fr/2012PEST1165

Van Leussen, W. (1994). Estuarine Macroflocs and Their Role in Fine-Grained Sediment Transport. *Ph. D. Thesis, University of Utrecht*. https://ci.nii.ac.jp/naid/10024267924/

van Maanen, B., & Sottolichio, A. (2018). Hydro- and sediment dynamics in the Gironde estuary (France): Sensitivity to seasonal variations in river inflow and sea level rise. *Continental Shelf Research*, *165*, 37–50. https://doi.org/10.1016/j.csr.2018.06.001

van Maren, D. S., & Cronin, K. (2016). Uncertainty in complex three-dimensional sediment transport models: Equifinality in a model application of the Ems Estuary, the Netherlands. *Ocean Dynamics*, *66*(12), 1665–1679. https://doi.org/10.1007/s10236-016-1000-9

van Maren, D. S., Winterwerp, J. C., & Vroom, J. (2015). Fine sediment transport into the hyper-turbid lower Ems River: The role of channel deepening and sediment-induced drag reduction. *Ocean Dynamics*, *65*(4), 589–605. https://doi.org/10.1007/s10236-015-0821-2

Vanney, J.-R. (1977). *Géomorphologie de la marge continentale sud-armoricaine* (Vol. 21). Société d'édition d'enseignement supérieur.

Vörösmarty, C. J., Meybeck, M., Fekete, B., Sharma, K., Green, P., & Syvitski, J. P. M. (2003). Anthropogenic sediment retention: Major global impact from registered river impoundments. *Global and Planetary Change*, *39*(1), 169–190. https://doi.org/10.1016/S0921-8181(03)00023-7

Waeles, B., Hir, P. L., & Lesueur, P. (2008). Chapter 32 A 3D morphodynamic process-based modelling of a mixed sand/mud coastal environment: The Seine estuary, France. In T. Kusuda, H. Yamanishi, J. Spearman, & J. Z. Gailani (Eds.), *Proceedings in Marine Science* (Vol. 9, pp. 477–498). Elsevier. https://doi.org/10.1016/S1568-2692(08)80034-4

Waeles, B., Le Hir, P., Lesueur, P., & Delsinne, N. (2007). Modelling sand/mud transport and morphodynamics in the Seine river mouth (France): An attempt using a process-based approach. *Hydrobiologia*, *588*(1), 69–82. https://doi.org/10.1007/s10750-007-0653-2

Willmott, C. J. (1981). On the Validation of Models. *Physical Geography*, *2*(2), 184–194. https://doi.org/10.1080/02723646.1981.10642213

Yang, S. L., Milliman, J. D., Li, P., & Xu, K. (2011). 50,000 dams later: Erosion of the Yangtze River and its delta. *Global and Planetary Change*, *75*(1), 14–20. https://doi.org/10.1016/j.gloplacha.2010.09.006

Zhang, G., Cheng, W., Chen, L., Zhang, H., & Gong, W. (2019). Transport of riverine sediment from different outlets in the Pearl River Estuary during the wet season. *Marine Geology*, *415*, 105957. https://doi.org/10.1016/j.margeo.2019.06.002

Appendix A: Willmott (1981) skill score

Model accuracy has been quantified using the skill score introduced by Willmott (1981) and commonly used in estuarine studies (Dunn et al., 2015; Toublanc et al., 2016; van Maanen & Sottolichio, 2018; van Maren et al., 2015). It compares the modelled (*Xmod*) and observed (*Xobs*) variations around the observed mean ($\overline{Xobs}$) as follows:

$$Skill = 1 - \frac{\sum |X_{mod} - X_{obs}|^2}{\sum \left(|X_{mod} - \overline{X_{obs}}| + |X_{obs} - \overline{X_{obs}}| \right)^2}$$

This skill score gives an index of agreement between the simulated and the measured variables between 0 and 1, an index of 1 indicating a perfect agreement and 0 meaning no correlation between the two variables. In complement to the correlation coefficient and the measure of the RMSE, it gives an idea of how error-free a model prediction is compared to the observation. Moreover, owing to its dimensionless nature, cross-comparisons for different model simulations can easily be done and interpreted.

Supplementary material:

Analysis of model stability and spin-up period

Sediment fluxes stability

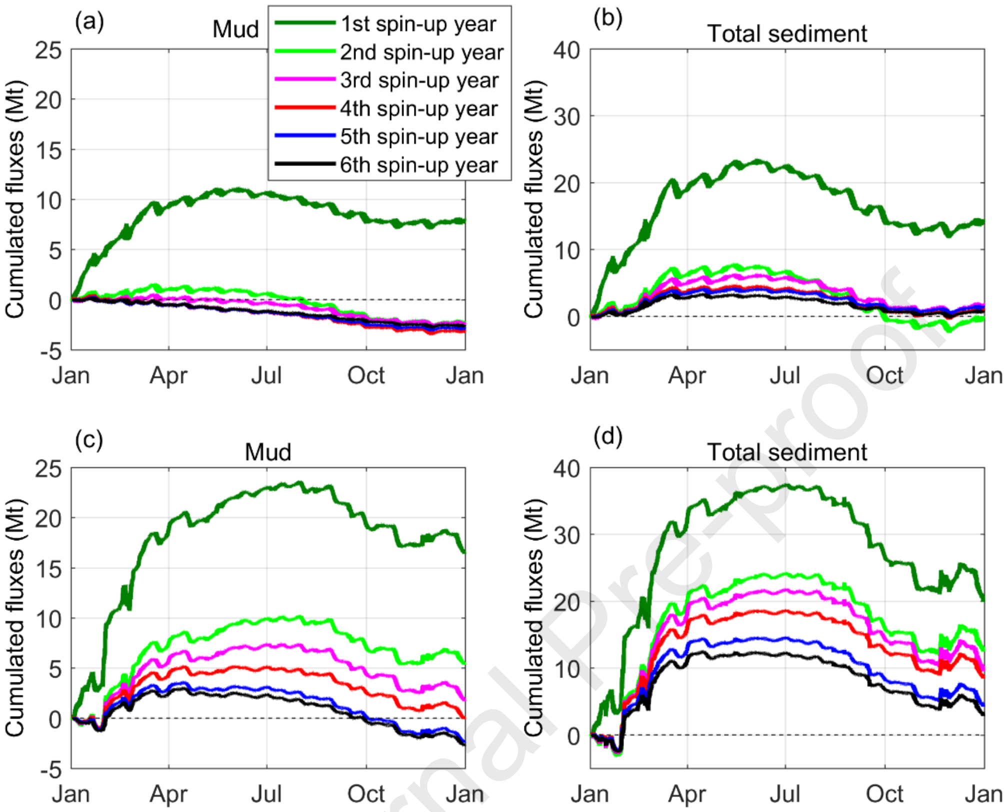

Figure 15 Time series of cumulative fluxes of (a, c) mud and (b, d) total sediment across sections (a, b) Verdon and (c, d) Isobath-25m (see Figure 1 for location) over the 6 simulated 2015 spin-up years.

Sediment distribution evolution

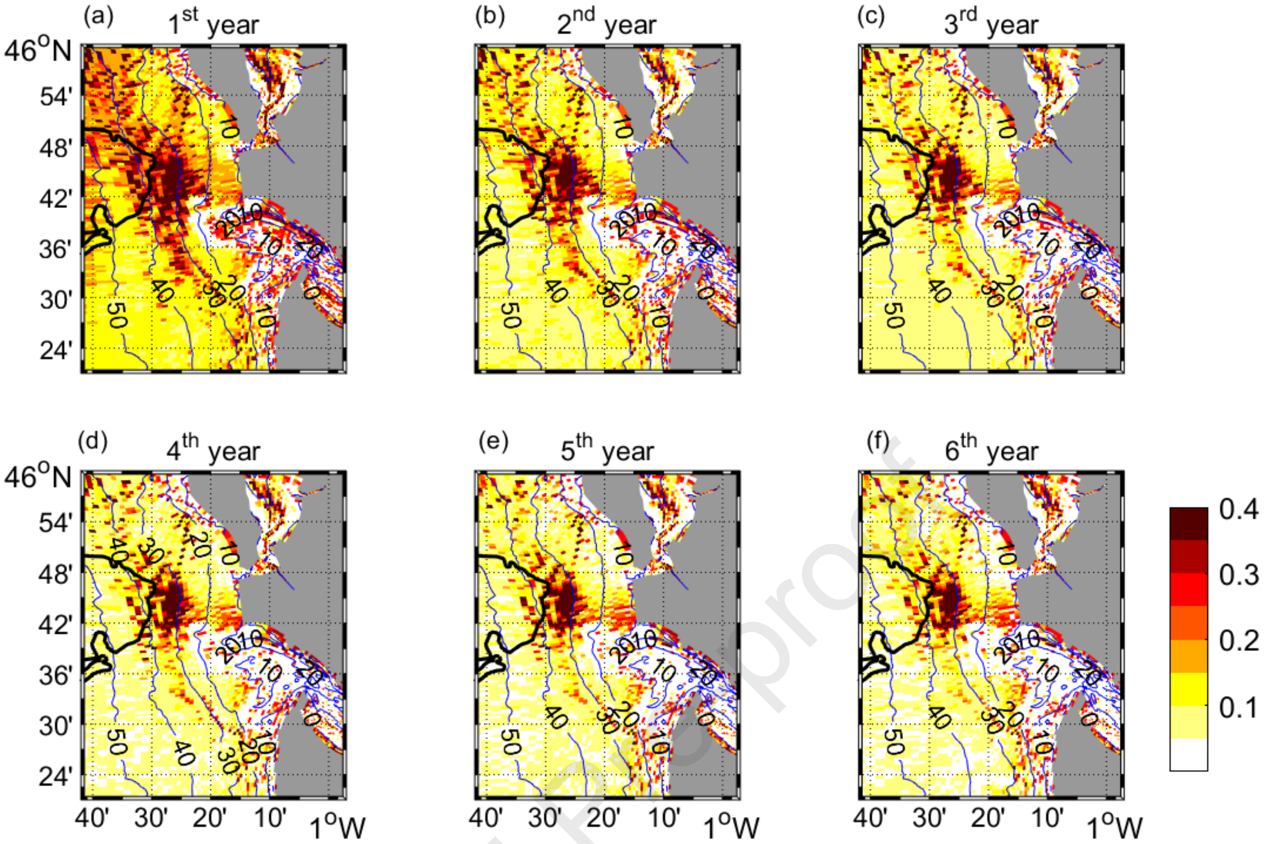

Figure 16: Mud fraction in the surficial sediment (11.6 cm) at the end of each simulated 2015 spin-up years. Blue contours are delimitating isobaths every 10 m (vertical reference: mean sea level). The black shape outlines the contour of the West Gironde Mud Patch (as drawn in Figure 1 based on Lamarque et al. (2021)).

ETM mass evolution

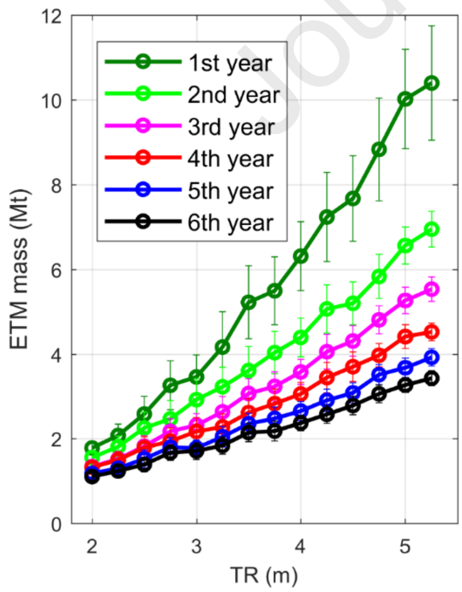

Figure 17 Estuarine Turbidity Maximum (ETM) mass in millions of tons as a function of the tidal range (TR) for the 6 simulated 2015 spin-up years.

Migration of the ETM with the river flow in the estuary

High river flow

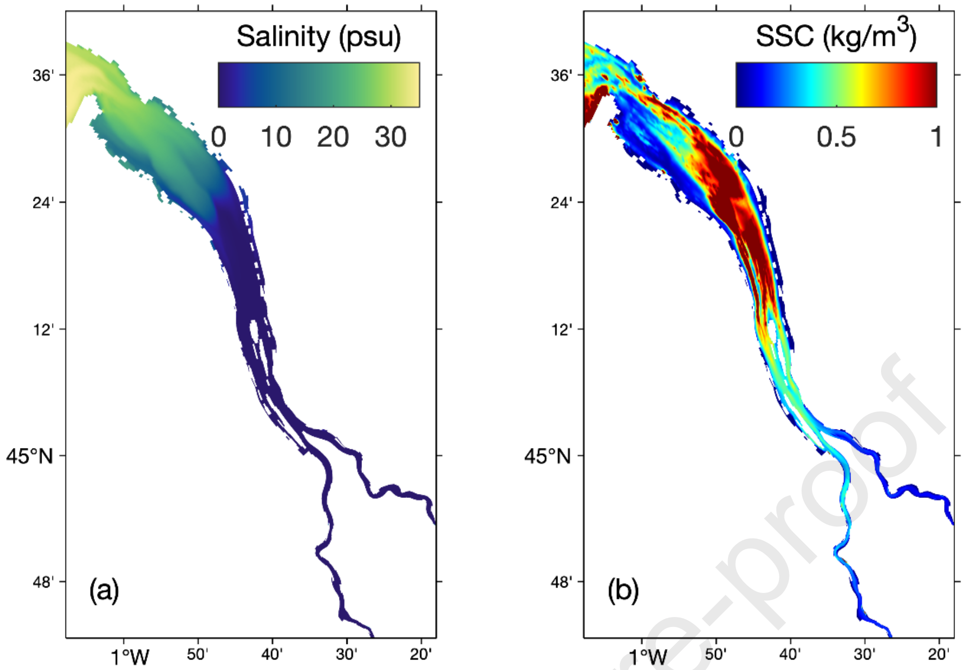

Low river flow

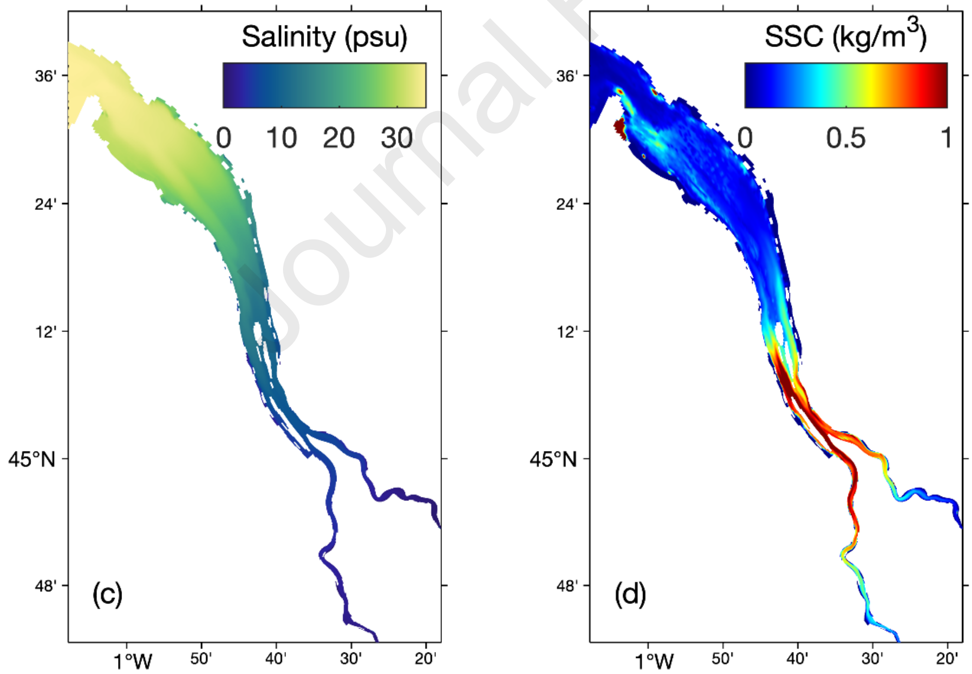

Figure 18 Near-bottom (1m above the bed) (a, c) salinity and (b, d) SSC outputs in (a, b) high river flow (February 2016) and (c, d) low river flow (August 2016). Turbidity fields are shown during neap tides and end of flood.

Behavior of the turbid plume at the estuarine mouth

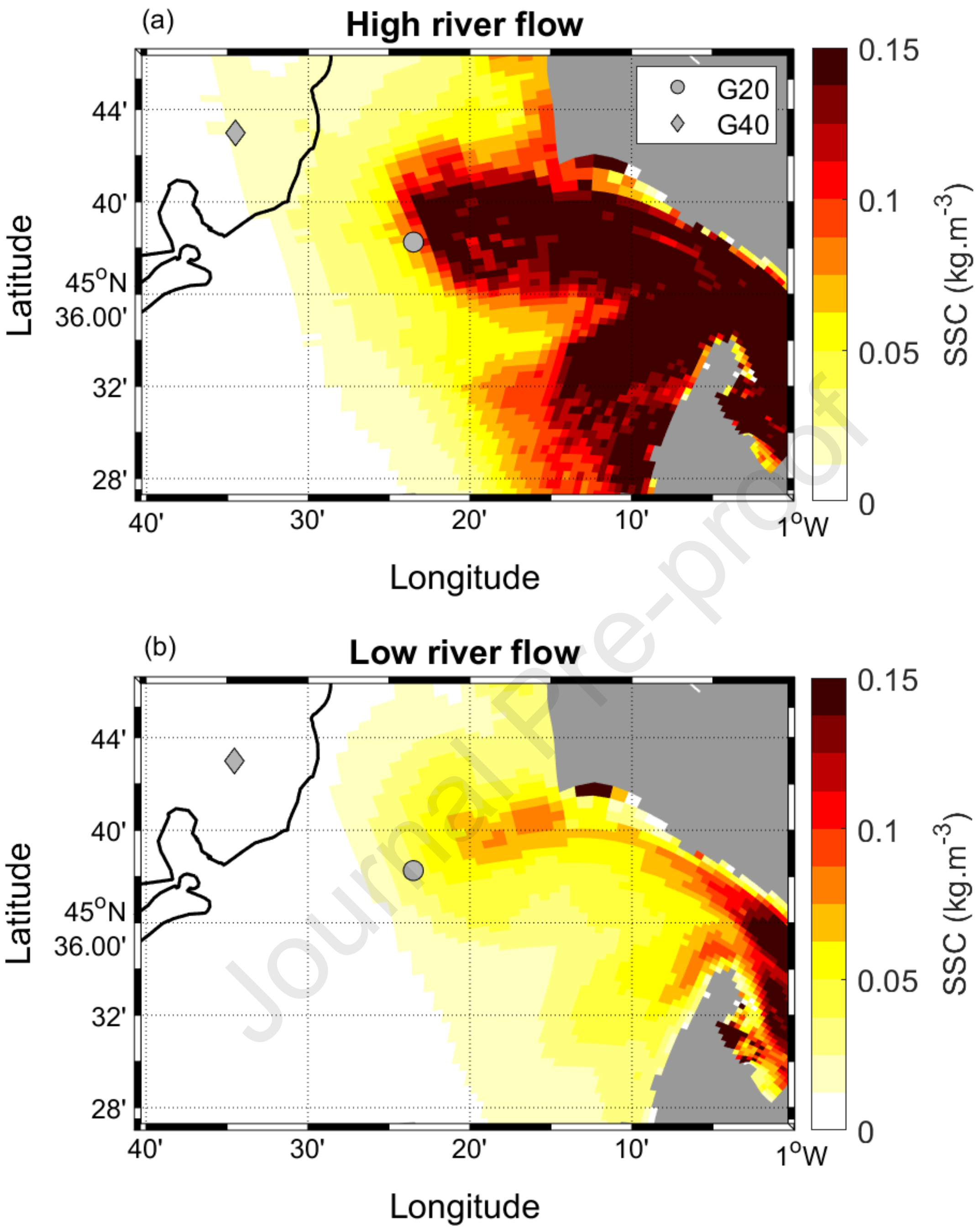

Figure 19: Horizontal variability of surface turbid plume off the estuarine mouth during (a) high and (b) low river discharge

Vertically-integrated residual sediment fluxes at the mouth

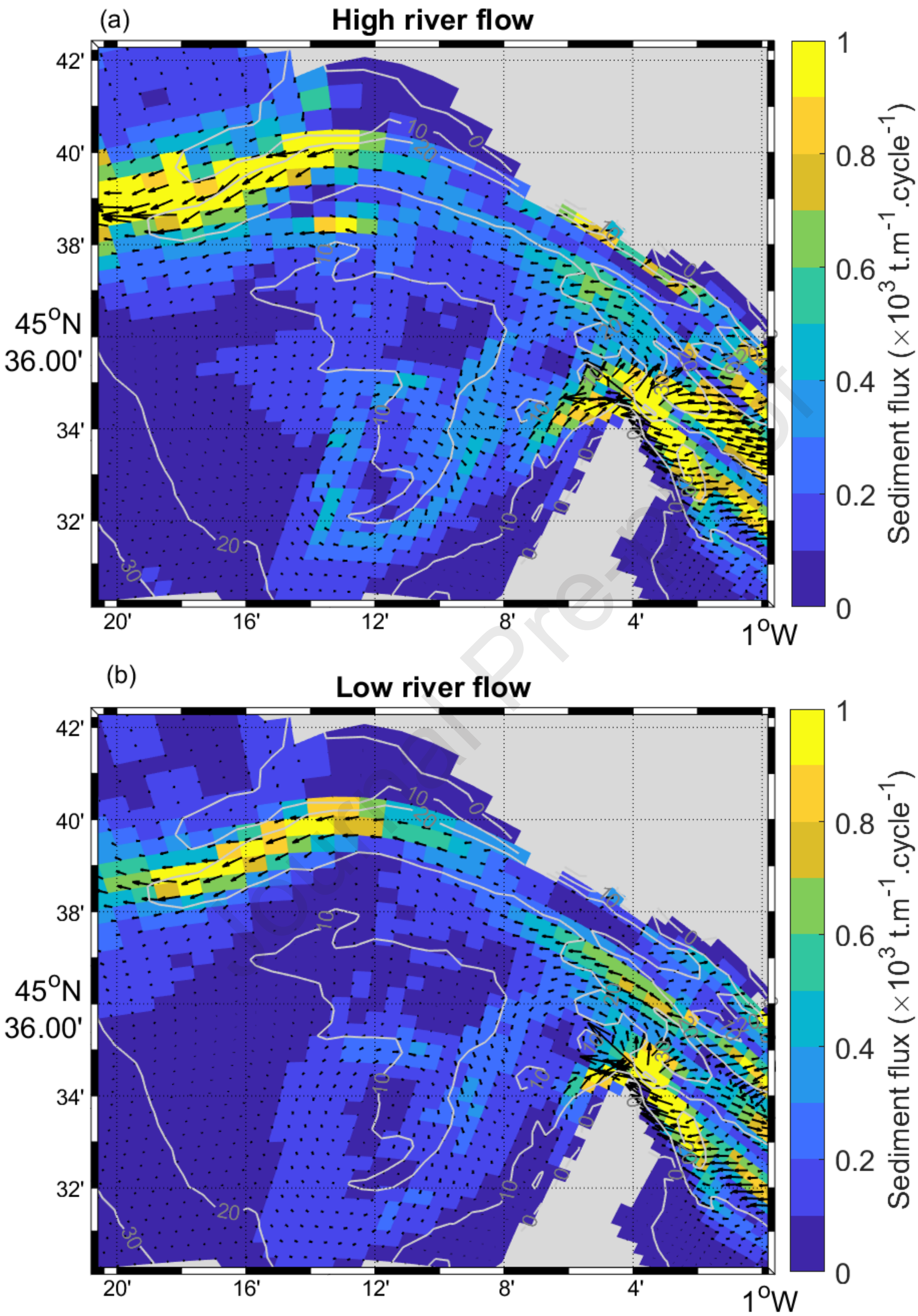

Figure 20: Vertically-integrated residual sediment fluxes through the estuarine mouth over a neap-spring cycle during (a) high and (b) low river discharge

Vertical profiles of longitudinal current and salinity at the mouth

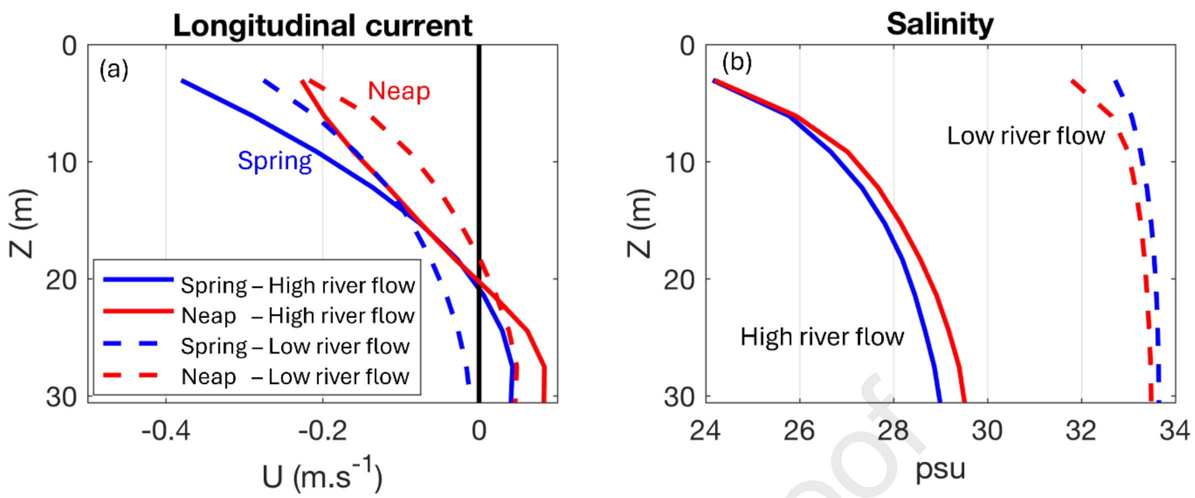

Figure 21 Vertical profiles of residual (a) longitudinal current and (b) salinity over one neap and one spring cycle of 7 days each, during both high and low river discharge conditions. Positive currents are directed upstream.

Highlights:

- A process-based model simulated mud/sand fluxes along an estuary-shelf continuum
- Density gradients drive up-estuary sand fluxes at the estuarine mouth
- The formation and dynamics of an active shelf mud deposition area are reproduced
- The trapping efficiency of the mudflat is modulated by waves and river turbid plume
- About 26% of the mud mass accumulated on the mudflat originates from the estuary

Declaration of interests

☒ The authors declare that they have no known competing financial interests or personal relationships that could have appeared to influence the work reported in this paper.

☐ The authors declare the following financial interests/personal relationships which may be considered as potential competing interests: